

BRL R 1801

BRL

AD

REPORT NO. 1801

12
13

BOUNDARY LAYER STUDIES ON A SPINNING
TANGENT - OGIVE - CYLINDER MODEL

Walter B. Sturek

July 1975

DDC
RECEIVED
SEP 12 1975
B

Approved for public release; distribution unlimited.

✓
USA BALLISTIC RESEARCH LABORATORIES
ABERDEEN PROVING GROUND, MARYLAND

ADA 014878

Secondary distribution of this report by originating or sponsoring activity is prohibited.

PROSECUTION for

NTIS	White Section	<input checked="" type="checkbox"/>
D.C.	Bluff Section	<input type="checkbox"/>
UNCLASSIFIED		<input type="checkbox"/>

CLASSIFICATION _____

DATE _____

BY _____

CLASSIFICATION AUTHORITY CODES _____

_____ OF SPECIAL _____

A

The findings in this report are not to be construed as an official Department of the Army position, unless so designated by other authorized documents.

SECURITY CLASSIFICATION OF THIS PAGE (When Data Entered)


✓ (Continued)

UNCLASSIFIED

SECURITY CLASSIFICATION OF THIS PAGE(When Data Entered)

20. ABSTRACT (Continued):

normal forces were measured using the strain-gage balance technique for different boundary layer configurations. These measurements revealed a substantial sensitivity of Magnus force to the boundary layer configuration. A preliminary comparison of the Magnus measurements to the theory of Vaughn and Reis yielded poor agreement. The data have been tabulated to facilitate their use in the evaluation of proposed theoretical models of the Magnus effect.



UNCLASSIFIED

SECURITY CLASSIFICATION OF THIS PAGE(When Data Entered)

TABLE OF CONTENTS

	<u>Page</u>
LIST OF ILLUSTRATIONS	5
I. INTRODUCTION	7
II. THE EXPERIMENT	7
A. Test Facility	7
B. Model	8
C. Optical Study	8
D. Strain-Gage Balance Measurements	8
III. DISCUSSION OF THE RESULTS	9
A. Effect of Spin on Boundary-Layer Transition	9
B. Magnus Force Measurements	10
C. Normal Force Measurements	11
IV. CONCLUDING REMARKS	11
REFERENCES	39
LIST OF SYMBOLS	41
DISTRIBUTION LIST	43

LIST OF ILLUSTRATIONS

<u>Figure</u>		<u>Page</u>
1.	View of Tangent-Ogive-Cylinder Model as Mounted in the Test Section of Supersonic Wind Tunnel No. 1	16
2.	Offset Struts Used in the Optical Study	17
3.	Spark Shadowgraph Showing Natural Boundary Layer Transition, $M = 2$, $\alpha = -4^\circ$, $Re_\ell = 8.8402 \times 10^6$	18
4.	Spark Shadowgraph Showing Boundary Layer Tripped Using a Band of No. 80 Sand Grit, $M = 2$, $\alpha = -4^\circ$, $Re_\ell = 8.7139 \times 10^6$	19
5.	Coordinate System Showing the Direction and Sense of Forces, Moments and Angles	20
6.	Boundary-Layer Transition Data	21
	a. $M = 2$, $\alpha = 2^\circ$	21
	b. $M = 2$, $\alpha = 4^\circ$	22
7.	Boundary-Layer Transition Data	23
	a. $M = 3$, $\alpha = 2^\circ$	23
	b. $M = 3$, $\alpha = 4^\circ$	24
8.	Boundary-Layer Transition Data	25
	a. $M = 4$, $\alpha = 2^\circ$	25
	b. $M = 4$, $\alpha = 4^\circ$	26
9.	Comparison of Magnus Force Measurements for Different Boundary Layer Configurations, $M = 3$	27
10.	a. Magnus Force Measurements for Low p_o , Natural Boundary-Layer Transition--Predominantly Laminar Boundary Layer, $M = 2$	28
	b. Magnus Force Measurements for High p_o , Natural Boundary-Layer Transition--Comparable Regions of Laminar and Turbulent Boundary Layer, $M = 2$	29
	c. Magnus Force Measurements for High p_o , Tripped Turbulent Boundary Layer, $M = 2$	30

LIST OF ILLUSTRATIONS (Continued)

<u>Figure</u>		<u>Page</u>
11.	a. Magnus Force Measurements for Low p_o , Natural Boundary-Layer Transition--Predominantly Laminar Boundary Layer, $M = 4$	31
	b. Magnus Force Measurements for High p_o , Natural Boundary-Layer Transition--Comparable Regions of Laminar and Turbulent Boundary Layer, $M = 4$	32
	c. Magnus Force Measurements for High p_o , Tripped Turbulent Boundary Layer, $M = 4$	33
12.	Comparison of Magnus Force Measurements to Theory, High p_o	34
	a. Natural Boundary-Layer Transition, $M = 3$, $\alpha = 4.42^\circ$.	34
	b. Tripped Turbulent Boundary Layer, $M = 3$, $\alpha = 4.42^\circ$.	35
13.	Normal Force Data	36
	a. $M = 2$	36
	b. $M = 3$	37
	c. $M = 4$	38

I. INTRODUCTION

Emphasis has recently been placed on obtaining increased range and greater payload capacity for new Army projectile shapes. These requirements have led to projectile shapes with long slender ogives, increased length and boattailed afterbodies. The new designs have resulted in decreased drag; however, the stability of these projectiles has also been decreased. Thus, these new shapes are more susceptible to a Magnus induced instability. Also, the increased length of these new shapes has contributed to an increase in the Magnus moment. These factors have resulted in renewed interest in the study of the Magnus effect.

This report describes an experimental study of the effects of spin on boundary-layer development over a seven caliber tangent-ogive-cylinder model in supersonic flow. This experimental study is part of the BRL Magnus research effort which is being undertaken to develop a better understanding of the physics of the Magnus effect. The objectives of this particular experiment are to: (1) examine the effect of spin on boundary-layer development; (2) examine the significance of the boundary-layer configuration (laminar, transitional or turbulent) on the resulting Magnus force experienced by the model; and (3) provide detailed experimental data which will be of value in evaluating theoretical models of the Magnus effect. This report is supplementary to Reference 1 which reports an experimental investigation of the flow over a spinning cone model.

II. THE EXPERIMENT

The experimental study consisted of two parts: (1) an optical study of the effects of spin on boundary-layer transition; and (2) the effect of different boundary-layer configurations on the Magnus force as measured using a strain-gage balance.

A. Test Facility

The test facility² used was Supersonic Tunnel No. 1 at the Ballistic Research Laboratories (BRL). This is a continuous flow facility with a flexible plate symmetric nozzle. The test section has a height of 38 cm

1. W. B. Sturek, "Boundary Layer Studies on a Spinning Cone," BRL Report No. 1649, U.S. Army Ballistic Research Laboratories, Aberdeen Proving Ground, Maryland, May 1973. AD 762564.
2. J. C. McMullen, "Wind Tunnel Testing Facilities at the Ballistic Research Laboratories," BRL Memorandum Report No. 1292, U.S. Army Ballistic Research Laboratories, Aberdeen Proving Ground, Maryland, July 1960. AD 244180.

and a width of 33 cm. The nominal tunnel operating conditions for each test are given in Table I. The total temperature was controlled within $\pm 1^\circ\text{K}$ and the total pressure was maintained within ± 0.4 percent during each individual test run.

B. Model

The model used for these tests was a seven caliber long tangent-ogive-cylinder with a one-caliber ogive section. The diameter of the cylinder portion was 5.08 cm. A view of the model mounted in the test section is shown in Figure 1. The model was suspended on ball bearings and an internal air driven turbine was used to drive the model in spin. The model was made of high strength aluminum alloy and was highly polished. The model was dynamically balanced to a tolerance of 2.1 gm-cm.

C. Optical Study

Spark shadowgraphs were taken of the flow over the model while mounted on an offset strut. Two offset struts were used giving angles of attack of 2° and 4° . A picture of these offset struts is shown in Figure 2. Using the roll head, pictures were taken at 15° increments in azimuth for azimuthal angles from 0 to $+180^\circ$ and from 0 to -90° . Spark shadowgraphs were obtained for $M = 2, 3$, and 4 and for spin rates of 0, 8,000, 16,000, and 24,000 rpm. The tunnel total pressure was maintained at a high value in order to enhance the occurrence of natural transition to turbulence before reaching the base of the model on the windside. The spark shadowgraphs were taken while holding the model at a constant spin rate. A spark shadowgraph of the flow over the model is shown in Figure 3 for $M = 2$, $\alpha = -4^\circ$, and $\omega = 0$ rpm.

D. Strain-Gage Balance Measurements

Magnus and normal forces were measured using the strain gage balance technique for different boundary-layer configurations. The boundary-layer configuration refers to the relative regions of laminar and turbulent boundary layer occurring on the model for a particular flow condition. The flow conditions obtained were: (1) low tunnel total pressure--predominantly laminar boundary layer; (2) high tunnel total pressure--approximately comparable regions of laminar and turbulent boundary layer (same operating conditions as that for the optical study); and (3) high tunnel total pressure with the boundary layer tripped to turbulent by a band of #80 sand grit, 0.63 cm wide, placed 2.5 cm from the tip of the model. The effectiveness of this trip is indicated in Figure 4 which shows a spark shadowgraph of the flow for $M = 2$, $\alpha = -4^\circ$, and $\omega = 0$. The boundary-layer trip performed well for the case shown here. At $M = 4$, the trip was somewhat less effective, but was considered satisfactory.

The strain gage balance used was SB219. This is a moment-type balance, designed and fabricated at the Exterior Ballistics Laboratory (EBL). This balance has three sets of gages: (1) forward normal, forward yaw; (2) aft normal, aft yaw; and (3) aft-aft yaw. The limiting loads are 60 in-lbs (6.78 m-N) in pitch and 43 in-lbs (4.86 m-N) in yaw at the forward position; 80 in-lbs (9.04 m-N) in pitch and 53 in-lbs (5.99 m-N) in yaw at the aft position; and 146 in-lbs (16.50 m-N) in yaw at the aft-aft position.

The Magnus measurements were made while holding the model at a fixed angle of attack. The model was spun up to 30,000 RPM using the internal air driven turbine, the turbine air was shut off, and data were recorded on magnetic tape at fixed intervals of time while the model coasted to zero spin. The spin down time was typically six minutes--very favorable for obtaining good quality Magnus data.

Normal force and moment data were obtained while the model was spinning, and also while the model was slowly moved in angle of attack from +12 to -4 degrees with zero spin.

The accuracy of the force measurements is estimated to be within $\pm .0006$ in side force coefficient and within $\pm .005$ in normal force coefficient.

III. DISCUSSION OF THE RESULTS

A. Effect of Spin on Boundary-Layer Transition

The location of boundary-layer transition was determined from the spark shadowgraphs as the position where the boundary layer appeared to be fully turbulent. An example of this determination is indicated in Figure 3. No attempt has been made to relate this criteria for transition to other means such as wall shear stress or wall heat transfer. It should be emphasized here that no attempt to relate the transition data obtained here to atmospheric flight will be made. These data are being obtained to better understand the influence of spin on boundary-layer development as it occurs on a wind tunnel model in order that a meaningful comparison can be made between calculations of Magnus effects and wind tunnel measurements. Figure 5 shows the coordinate system used in presenting the data along with the direction and sense of the forces, moments, and angles.

The boundary-layer transition data are shown in Figures 6 through 8. The data are plotted as the distance in calibers from the base of the model to the location of boundary-layer transition. A solid line has been drawn to indicate what is felt to be the trend of the data. The cross-hatched region represents the region of turbulent boundary layer while the clear region represents laminar boundary layer.

The data indicate substantial scatter for some cases. This is especially true for the $M = 2$ data. The cause of this excessive scatter is believed to be linked with the intermittent unsteady diffuser flow that occurred at $M = 2$. However, for the most part, a trend of the data as a function of azimuthal position and spin rate is apparent. The trend for the data shown in Figure 7a is particularly well defined. The trends with spin are: (1) transition is delayed where the crossflow velocity is in the same direction as the surface spin; and (2) transition occurs earlier where the crossflow velocity opposes the spin velocity.

The peculiar dip in the trend of the data for $\phi \approx 180^\circ$ is sufficiently persistent to lead one to suspect that this observation is not experimental uncertainty. In considering the physics of this three-dimensional boundary layer flow, it is apparent that $\phi = 180^\circ$ is a rear stagnation point in the crossflow plane. Although the inviscid azimuthal velocity is zero at this position, the azimuthal velocity derivative is not zero and the flow is turned as it approaches this crossflow stagnation point. The unusual behavior of the transition location at the $\phi \approx 180^\circ$ position is likely a manifestation of this flow situation.

B. Magnus Force Measurements

A comparison of Magnus force measurements is shown in Figure 9 for the $M = 3$ data. These data are plotted as side force coefficient versus non-dimensional spin rate for the three different boundary-layer configurations. The significant trends of the data are: (1) the low p_o ($Re_D = 0.59 \times 10^6$) data--predominantly laminar boundary layer--are nonlinear with spin rate and greater in magnitude than the high p_o ($Re_D = 1.06 \times 10^6$) data with natural boundary-layer transition; (2) the high p_o data, with and without the boundary-layer trip, are linear with spin rate; and (3) the tripped turbulent boundary layer data are greater in magnitude at all spin rates than either case with natural boundary layer transition.

Additional examples of the Magnus force measurements are shown in Figures 10 and 11 for $M = 2$ and 4. These data exhibit trends similar to that described above. A complete tabulation of the force measurements and boundary layer transition data is given in Table II.

The only theory presently available for predicting Magnus effects on bodies of revolution in supersonic flow is that published by Vaughn and Reis³. This theory is a semi-empirical approach and attempts to

3. H. R. Vaughn and G. E. Reis, "A Magnus Theory for Bodies of Revolution," SC-RR-72 0537, Sandia Laboratories, Albuquerque, New Mexico, January 1973; also, AIAA Journal, Vol. 11, No. 10, p. 1396, October 1973.

include the effects of vortex formation, centrifugal pressure distribution and boundary-layer transition on the Magnus force experienced by the spinning projectile in addition to the conventional contribution of asymmetric boundary-layer development. The theory is presented as closed form solutions for Magnus force and moment for several body configurations. The closed form solutions for an ogive-cylinder body have been taken directly from Reference 3 and the data of this experiment used as input to calculate Magnus force and moment.

Two examples are shown in Figures 12a and 12b comparing the calculated and experimental Magnus force for two different boundary-layer configurations. The data are plotted as Magnus force coefficient versus spin rate. In Figure 12a--high p_o with natural transition--the theory is approximately 60% greater in absolute value than the experiment. The theory indicates nonlinearity with spin similar to that indicated in the experimental data. In Figure 12b--high p_o with tripped boundary layer--the theory is greater in absolute value than the experiment by almost 200%. Thus, it is seen that Vaughn's theory overpredicts the Magnus force and is overly sensitive to boundary-layer configuration, at least for the results considered here. These results are typical of comparisons made utilizing all the data tabulated in Table II.

C. Normal Force Measurements

Examples of the normal force measurements are shown in Figures 13a-c. The data are plotted as normal force coefficient versus angle of attack, and were obtained as the model was slowly pitched in angle of attack from $+12^\circ$ to -4° while the model was not spinning. These data are linear for $\alpha \leq 4^\circ$. For $\alpha > 4^\circ$, the data become increasingly nonlinear indicating the increasing influence of vortex formation on the surface pressure distribution. These data also indicate that the normal force coefficient is relatively insensitive to Reynolds number and boundary-layer configuration.

IV. CONCLUDING REMARKS

An experimental investigation of the effects of surface spin on boundary-layer development and Magnus force for a seven caliber tangent-ogive-cylinder model with a one-caliber ogive at $M = 2, 3$, and 4 has been reported.

The data indicate that boundary-layer transition is affected by spin in a manner consistent with the physical picture of the flow. It has also been shown that Magnus force is significantly influenced by the boundary-layer configuration. These data strengthen the need for a good theoretical model of the effects of surface spin on boundary-layer development in order for Magnus effects to be calculated with sufficient confidence to be useful in projectile design.

The data from this experiment have been tabulated to facilitate their usefulness in evaluating theoretical models of Magnus. A preliminary comparison of these data with Vaughn's theory indicated that the theory overpredicted the Magnus force and was overly sensitive to the boundary-layer configuration.

Table I. Wind Tunnel Nominal Operating Conditions

<u>M</u>	<u>$p_o, N/M^2 \times 10^{-6}$</u>	<u>$T_o, ^\circ K$</u>	<u>Test Type</u>	<u>Config.</u>	<u>$Re_D \times 10^{-6}$</u>
2	.214	310	Optical	10	1.26
2	.107	310	Force	10	0.63
2	.214	310	Force	10	1.26
2	.214	310	Force	20	1.26
3	.300	310	Optical	10	1.06
3	.167	310	Force	10	0.59
3	.300	310	Force	10	1.06
3	.300	310	Force	20	1.06
4	.504	310	Optical	10	1.06
4	.372	310	Force	10	0.79
4	.504	310	Force	10	1.06
4	.504	310	Force	20	1.06

NOTE: Configuration (CONFIG.) = 10, basic model without boundary layer trip

= 20, basic model with boundary layer trip consisting of a .63 cm wide band of #80 sand grit placed 2.5 cm from the model leading edge

TABLE II. TABULATED FORCE AND BOUNDARY LAYER TRANSITION DATA

RUN	M	ALPHA	PO	TO	A	CY	H	C	CYM	D	REL	BOUNDARY-LAYER	LEE	WIND	CN	CM	MCP
121.0	2.0	1.20	.214	310.0	-.009161		.000000	-.023890		.000000	8.8577		.261	.757	.0619	.3541	5.72
122.0	2.0	2.42	.214	311.0	-.024480		.000000	-.033410		.000000	8.8319		.298	.803	.1234	.7106	5.76
123.0	2.0	4.82	.214	312.0	-.058940		.028050	-.059790		.022520	8.7538		.273	.931	.2555	1.4475	5.67
124.0	2.0	7.21	.214	311.0	-.110300		.025070	-.097700		-.007631	8.7825		.249	1.000	.4121	2.2547	5.47
126.0	2.0	-1.20	.214	310.0	-.009328		.000000	.035870		.000000	8.8395		.261	.603	-.0581	-.3465	5.96
127.0	2.0	-2.43	.213	310.0	.026360		.023280	.021530		.134200	8.8411		.273	.507	-.1207	-.7081	5.87
128.0	2.0	-4.83	.214	310.0	.055280		.000000	.073040		.000000	8.8402		.347	.537	-.2496	-1.4396	5.77
132.0	2.0	1.09	.107	310.0	-.029890		.033550	.001320		-.057930	4.4215		.715	.926	.0574	.3392	5.91
133.0	2.0	2.20	.107	310.0	-.056140		.075700	-.030910		.010160	4.4254		.695	1.000	.1120	.6657	5.94
134.0	2.0	4.38	.107	310.0	-.082710		.077170	-.114600		.090960	4.4145		.606	1.000	.2321	1.3336	5.75
135.0	2.0	6.58	.107	310.0	-.150600		.146500	-.169700		.034050	4.4242		.571	1.000	.3691	2.0638	5.59
136.0	2.0	8.74	.107	310.0	-.214500		.067340	-.214100		-.121100	4.4134		.562	1.000	.5398	2.8758	5.33
137.0	2.0	10.88	.107	310.0	-.226800		.0219400	-.246500		-.152000	4.4071		.557	1.000	.7604	3.8106	5.01
138.0	2.0	-1.07	.107	310.0	-.037800		-.101700	-.013980		.174300	4.4094		.746	.921	-.0484	-.2859	5.90
139.0	2.0	-2.19	.107	310.0	.058940		-.120400	.026520		.087280	4.4123		.679	1.000	-.1047	-.6181	5.90
140.0	2.0	-4.38	.107	310.0	.079110		-.076730	.106700		.022090	4.4138		.616	.874	-.2202	-1.2912	5.86
142.0	3.0	1.12	.300	311.0	-.012000		.000000	-.017340		.000000	7.4376		.544	.913	.0593	.3222	5.43
143.0	3.0	2.22	.300	312.0	-.026420		.013170	-.040820		.026160	7.4264		.557	.988	.1233	.6616	5.37
144.0	3.0	4.42	.299	312.0	-.061350		.042910	-.086960		.058280	7.4222		.569	1.000	.2222	1.3592	5.18
145.0	3.0	6.61	.300	313.0	-.143400		.170800	-.124300		-.003151	7.4104		.557	1.000	.4324	2.1236	4.91
146.0	3.0	8.72	.299	313.0	-.218500		.235700	-.138400		-.196500	7.3836		.000	.000	.6431	2.9388	4.57
147.0	3.0	-1.12	.299	313.0	.012900		.000000	.023860		.000000	7.3815		.757	.569	-.0650	-.3536	5.44
148.0	3.0	-2.26	.299	313.0	.025220		.000000	.042160		.000000	7.3699		.655	.581	-.1298	-.6984	5.38
149.0	3.0	-4.46	.299	313.0	.064130		-.039260	.088260		-.015570	7.3717		.557	.586	-.2702	-1.4032	5.19
156.0	3.0	1.07	.167	312.0	-.013730		.000000	-.033240		.000000	4.1489		.865	1.000	.0596	.3140	5.27
157.0	3.0	2.11	.167	312.0	-.035540		.035980	-.084440		.115200	4.1429		.815	1.000	.1219	.6440	5.28
158.0	3.0	4.24	.167	312.0	-.088830		.132400	-.218200		.397000	4.1303		.746	1.000	.2571	1.3260	5.16
159.0	3.0	6.34	.167	312.0	-.158800		.222400	-.305100		.335300	4.1263		.704	1.000	.4178	2.0460	4.90
160.0	3.0	8.39	.167	312.0	-.150100		-.027230	-.293800		-.058610	4.1334		.631	1.000	.6256	2.8459	4.55
161.0	3.0	-1.04	.167	312.0	.012120		.000000	.031540		.000000	4.1293		.872	.588	-.0562	-.3055	5.43
162.0	3.0	-2.11	.167	313.0	.025920		.000000	.067830		.000000	4.1267		.833	1.000	-.1173	-.6305	5.38
163.0	3.0	-4.24	.167	312.0	.086790		-.117100	.215400		-.363900	4.1315		.724	1.000	-.2510	-1.3040	5.20
166.0	4.0	1.08	.504	310.0	-.011960		.000000	-.035620		.000000	7.4693		.815	.975	.0579	.3042	5.25
167.0	4.0	2.13	.503	311.0	-.022800		.000000	-.062000		.000000	7.4238		.791	1.000	.1208	.6162	5.10
168.0	4.0	4.26	.504	311.0	-.063100		.066650	-.128800		.140300	7.4327		.616	1.000	.2571	1.2596	4.90
169.0	4.0	6.37	.504	311.0	-.107400		.121900	-.170400		.091560	7.4278		.603	1.000	.4174	1.9425	4.65
170.0	4.0	-1.06	.504	311.0	.010110		.000000	.027010		.000000	7.4280		.699	1.000	-.0623	-.3151	5.06
171.0	4.0	-2.12	.504	311.0	.021410		.000000	.053450		.000000	7.4228		.741	1.000	-.1250	-.6278	5.02
172.0	4.0	-4.25	.505	311.0	.060830		-.049910	.123100		-.144100	7.4210		.678	1.000	-.2604	-1.2682	4.87
179.0	4.0	1.02	.373	308.0	-.010360		.000000	-.043100		.000000	5.5610		.853	1.000	.0435	.2169	4.99
180.0	4.0	2.08	.372	309.0	-.031730		.042250	-.098400		.127900	5.5293		.853	1.000	.1071	.5311	4.96
181.0	4.0	4.17	.372	309.0	-.069770		.083110	-.159400		.132500	5.5453		.776	1.000	.2396	1.1568	4.83
182.0	4.0	6.24	.372	309.0	-.118900		.145700	-.234600		.202000	5.5505		.660	1.000	.2974	1.8259	4.59
183.0	4.0	-1.05	.372	309.0	.011400		.000000	.044900		.000000	5.5252		.850	1.000	-.0751	-.3753	5.00
184.0	4.0	-4.20	.372	309.0	.071110		-.079040	.161400		-.142300	5.5408		.840	1.000	-.2693	-1.3057	4.85

RUN	M	ALPHA	PO	TC	A	CY	S	C	CYM	D	KEL	LEF	WINT	CN	CV	ICP
193.0	4.0	1.06	.505	310.0	-.012830	.000000	.000000	-.021630	.000000	.000000	7.0010	.000	.000	.0552	.2870	5.21
195.0	4.0	4.26	.505	310.0	-.061480	.000000	.000000	-.088310	.000000	.000000	7.4627	.000	.000	.2496	1.2248	4.91
196.0	4.0	6.36	.504	311.0	-.106960	.000000	.000000	-.141800	.000000	.000000	7.4275	.000	.000	.4091	1.8950	4.64
197.0	4.0	-1.06	.504	311.0	.012800	.000000	.000000	.020590	.000000	.000000	7.4182	.000	.000	-.0606	-.3038	5.01
198.0	4.0	-2.14	.502	311.0	.026940	.000000	.000000	.044090	.000000	.000000	7.3925	.000	.000	-.1214	-.6117	5.51
199.0	4.0	-4.24	.504	311.0	.060690	.000000	.000000	.089070	.000000	.000000	7.4153	.000	.000	-.2522	-1.2291	4.87
203.0	3.0	1.09	.300	313.0	-.015850	.000000	.000000	-.020550	.000000	.000000	7.3976	.000	.000	.0561	.3028	5.40
204.0	3.0	2.20	.300	314.0	-.032890	.000000	.000000	-.042150	.000000	.000000	7.3873	.000	.000	.1200	.6292	5.33
205.0	3.0	4.42	.300	314.0	-.078090	.000000	.000000	-.094450	.000000	.000000	7.3835	.000	.000	.2586	1.3290	5.14
209.0	3.0	6.59	.299	310.0	-.136700	.000000	.000000	-.155500	.000000	.000000	7.5461	.000	.000	.4253	2.0711	4.86
210.0	3.0	-1.11	.300	312.0	.014960	.000000	.000000	.030060	.000000	.000000	7.4448	.000	.000	-.0640	-.3414	5.33
211.0	3.0	-2.23	.299	313.0	.032380	.000000	.000000	.055950	.000000	.000000	7.4093	.000	.000	-.1267	-.6735	5.31
212.0	3.0	-4.45	.300	313.0	.077870	.000000	.000000	.109000	.000000	.000000	7.3895	.000	.000	-.2641	-1.3542	5.15
215.0	2.0	1.18	.214	313.0	-.015830	.000000	.000000	-.024000	.000000	.000000	8.7373	.000	.000	.0596	.3394	5.70
216.0	2.0	2.39	.214	313.0	-.035190	.000000	.000000	-.043060	.000000	.000000	8.7395	.000	.000	.1193	.6891	5.75
217.0	2.0	4.80	.214	313.0	-.086250	.000000	.000000	-.095040	.000000	.000000	8.7242	.000	.000	.2516	1.4207	5.61
218.0	2.0	7.17	.214	313.0	-.155600	.000000	.000000	-.169600	.000000	.000000	8.7265	.000	.000	.4087	2.2108	5.41
219.0	2.0	-1.21	.214	313.0	.013660	.000000	.000000	.037990	.000000	.000000	8.7391	.000	.000	-.0577	-.3484	6.03
220.0	2.0	-2.43	.214	313.0	.033840	.000000	.000000	.059500	.000000	.000000	8.7139	.000	.000	-.1185	-.7004	5.91
221.0	2.0	-4.82	.214	313.0	.086530	.000000	.000000	.117900	.000000	.000000	8.7139	.000	.000	-.2487	-1.4315	5.76

BOUNDARY-LAYER

EXPLANATION-

M=MACH NUMBER

ALPHA=ANGLE OF ATTACK, DEGREES

PO=TUNNEL TOTAL PRESSURE, PASCALS*10E-6

TC=TUNNEL TOTAL TEMPERATURE, DEGREES KELVIN

CY=SIDE FORCE COEFFICIENT, $CY = A(PD/VI) + B(PD/VI)^2$

CYM=SIDE FORCE COEFFICIENT, $CYM = C(PD/VI) + D(PD/VI)^2$

REL=REYNOLDS NUMBER BASED ON MODEL LENGTH*10E-6

BOUNDARY LAYER(LEE,WIND)=POSITION OF BOUNDARY LAYER TRANSITION AS

DISTANCE FROM MODEL LEADING EDGE DIVIDED BY THE MODEL LENGTH.

TRANSITION LOCATION DETERMINED FROM SPARK SHADOWGRAPHS OF FLOW

OVER UNSPINNING MODEL. EQUALS ZERO FOR TRIPPED BOUNDARY LAYER,

EQUALS 1.0 FOR BOUNDARY LAYER REMAINING LAMINAR TO BASE OF MODEL.

CN=NORMAL FORCE COEFFICIENT

CM=PITCHING MOMENT COEFFICIENT

NCP=LOCATION OF CENTER OF PRESSURE, NCP=CM/CN

ALL MOMENTS ARE REFERENCED TO THE MODEL BASE

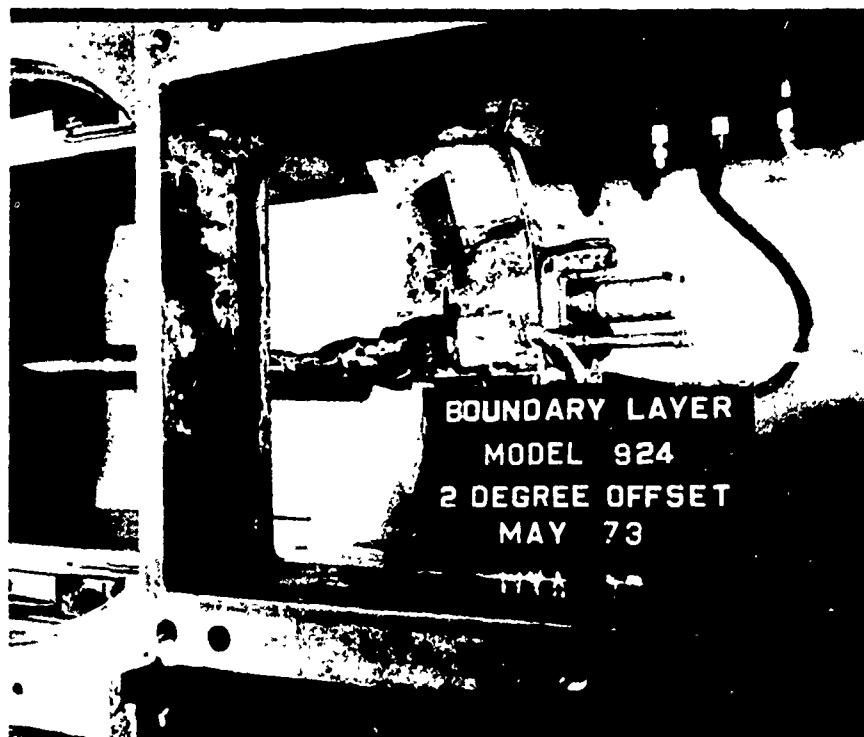
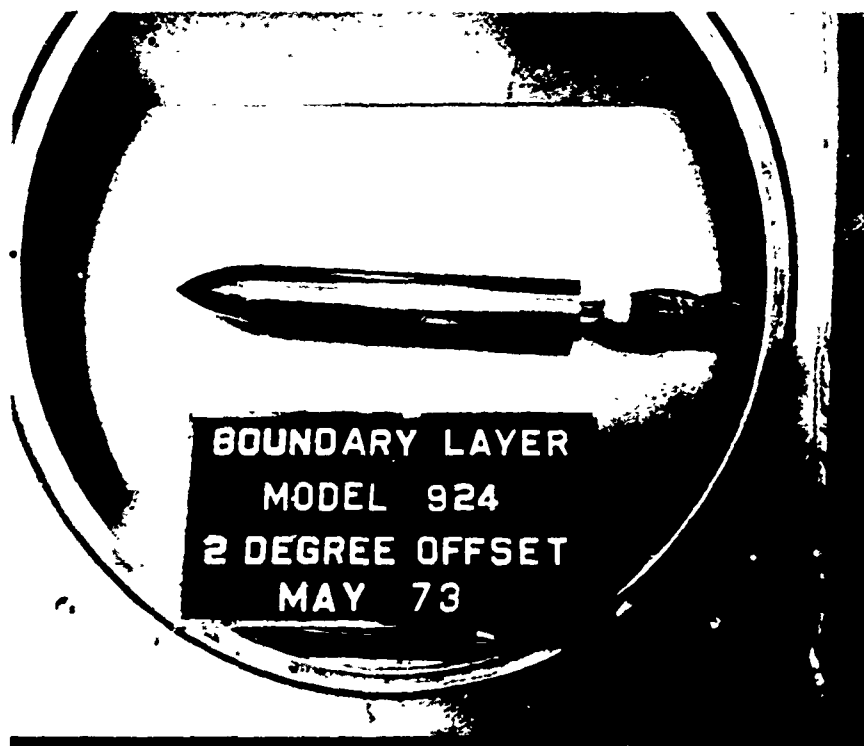


Figure 1. View of Tangent-Ogive-Cylinder Model as Mounted in the Test Section of Supersonic Wind Tunnel No. 1

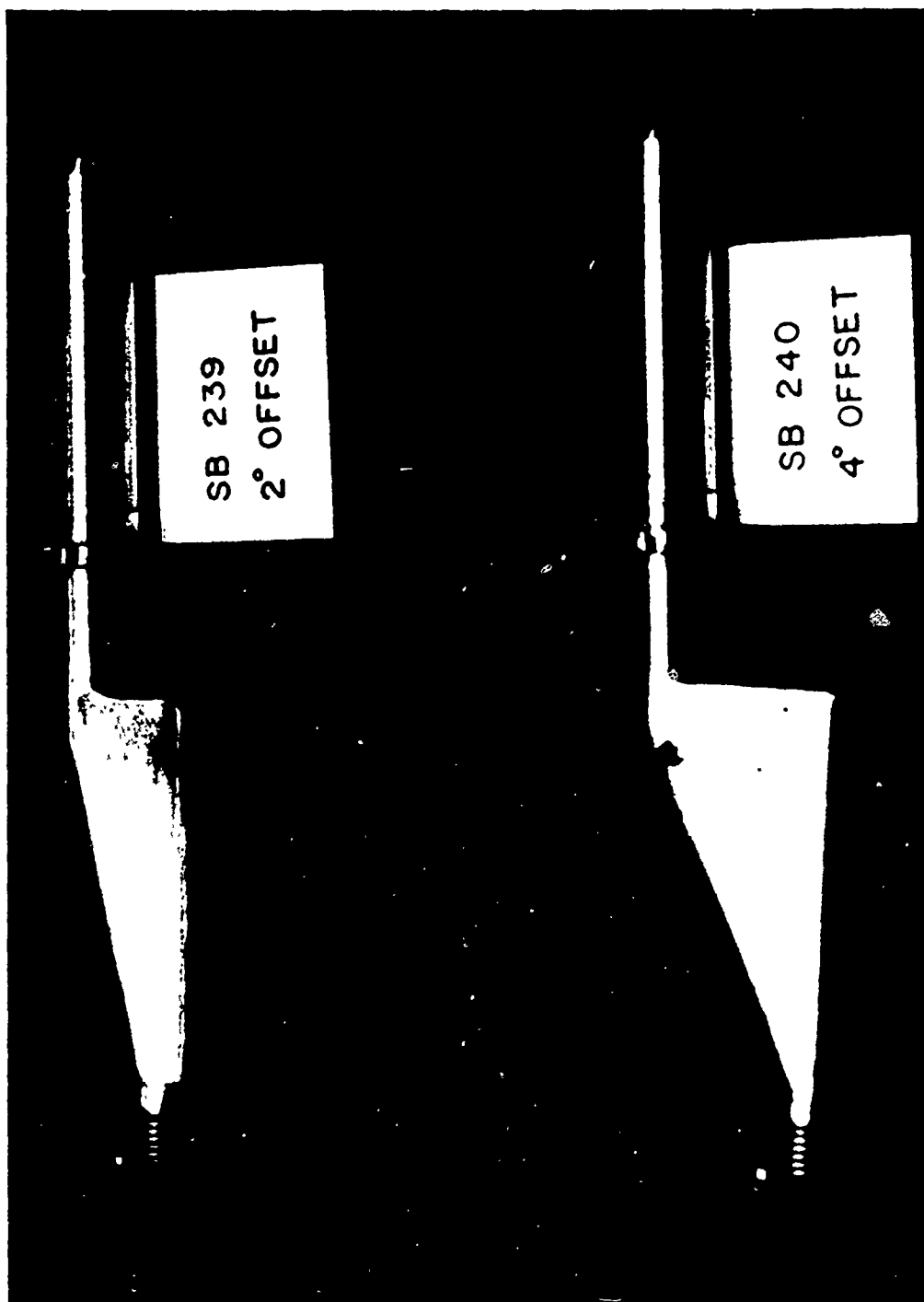


Figure 2. Offset Struts Used in the Optical Study

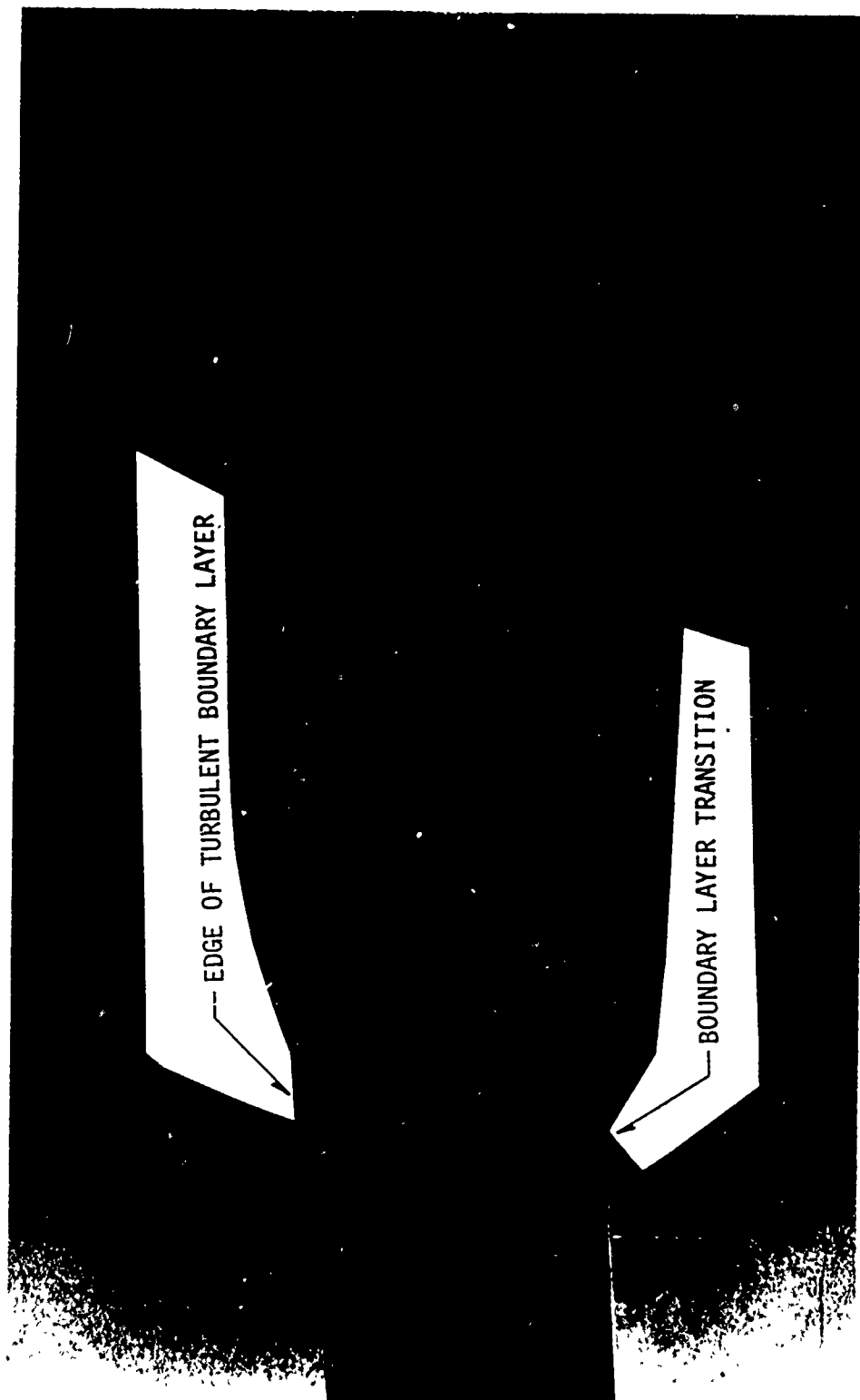


Figure 3. Spark Shadowgraph Showing Natural Boundary Layer Transition,
 $M = 2$, $\alpha = -4^\circ$, $Re_\rho = 8.8402 \times 10^6$

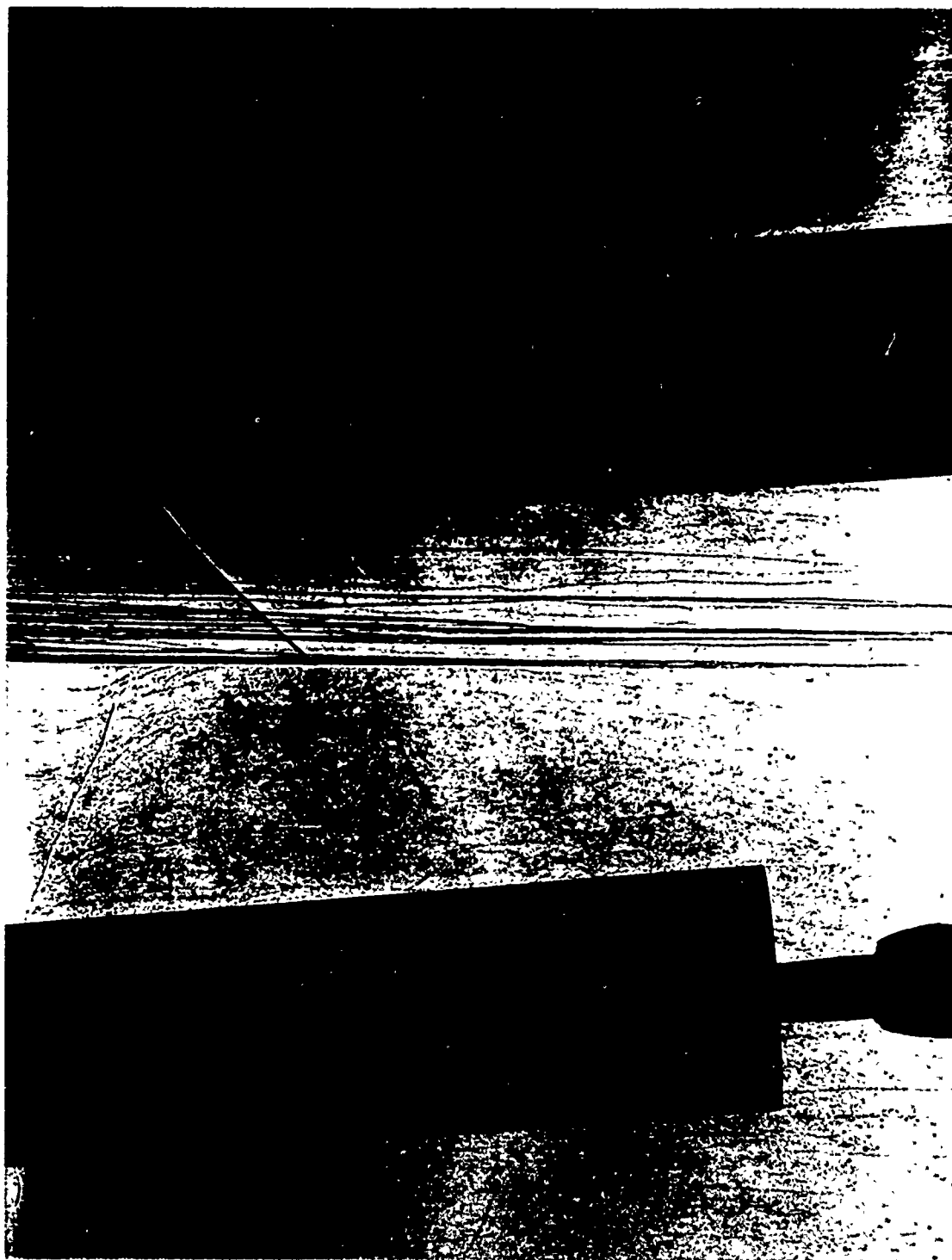


Figure 4. Spark Shadowgraph Showing Boundary Layer Tripped
Using a Band of No. 80 Sand Grit, $M = 2$, $\alpha = -4^\circ$,
 $Re_\ell = 8.7139 \times 10^6$

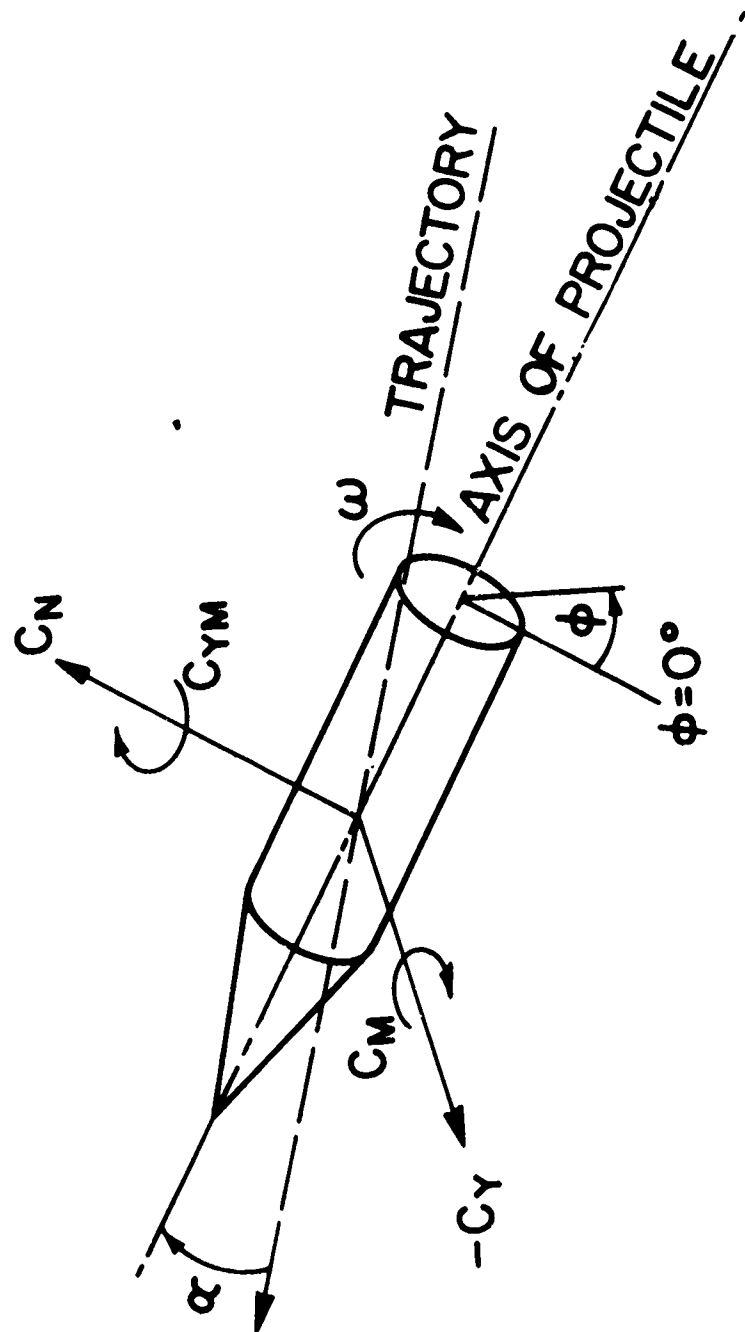


Figure 5. Coordinate System Showing the Direction and Sense of Forces, Moments and Angles

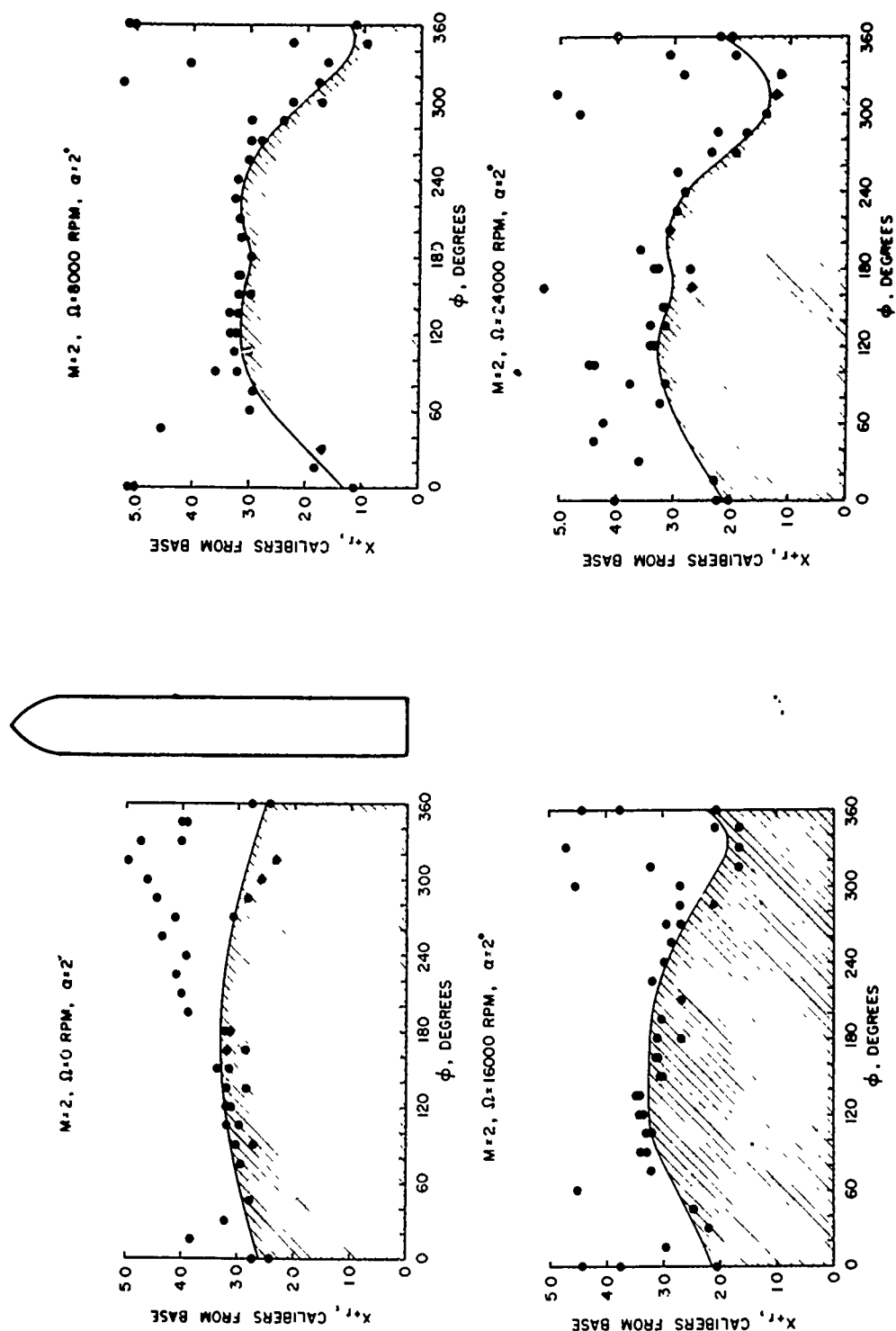


Figure 6. Boundary Layer Transition Data

a. $M = 2, \alpha = 2^\circ$

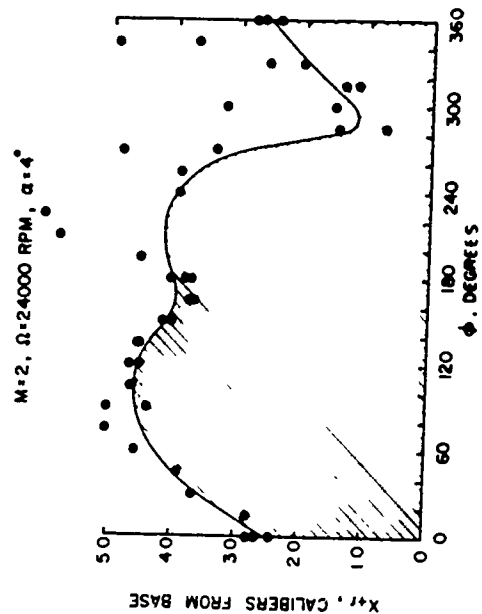
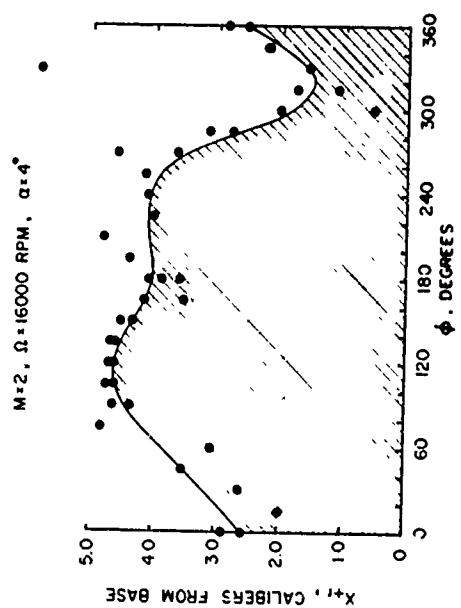
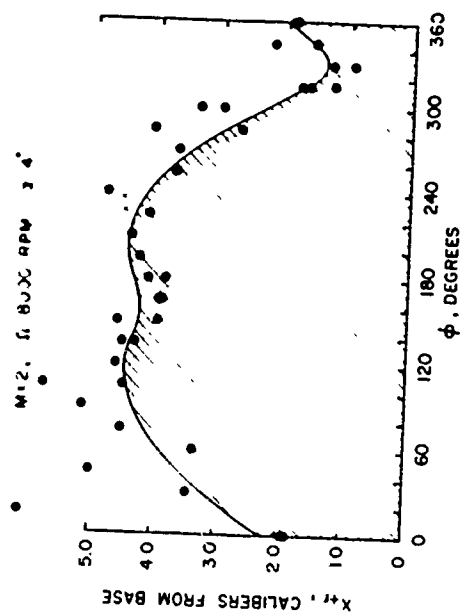
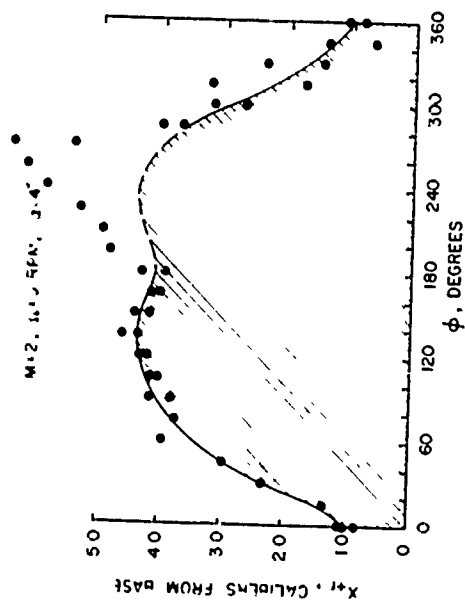
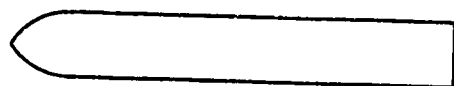


Figure 6. Concluded

b. $M = 2, \alpha = 4^\circ$

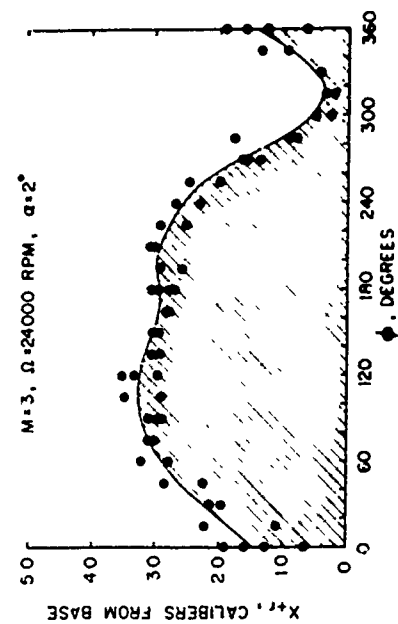
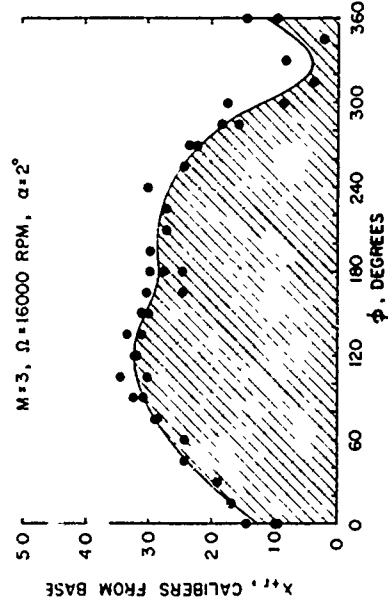
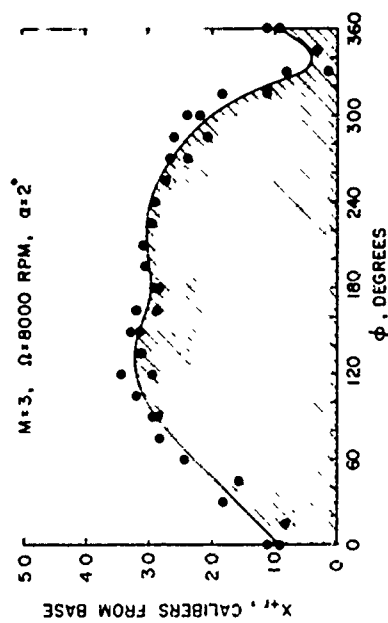
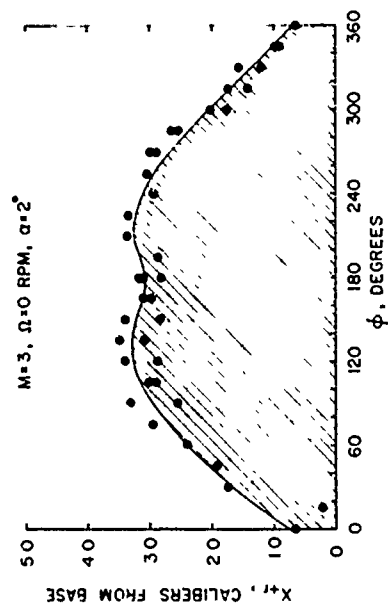
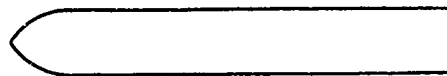
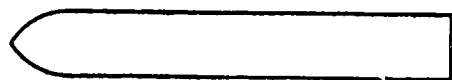
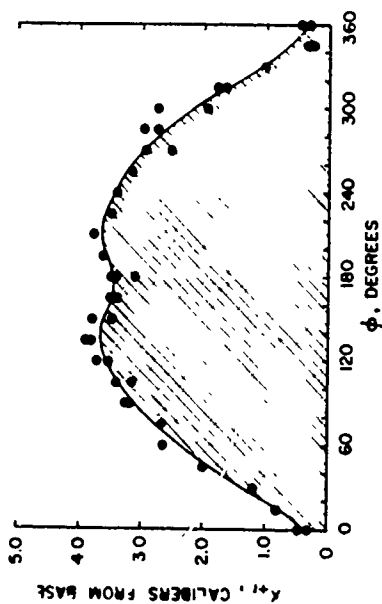


Figure 7. Boundary Layer Transition Data

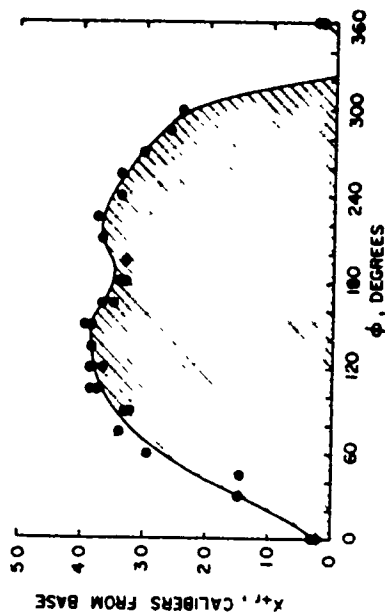
a. $M = 3, \alpha = 2^\circ$



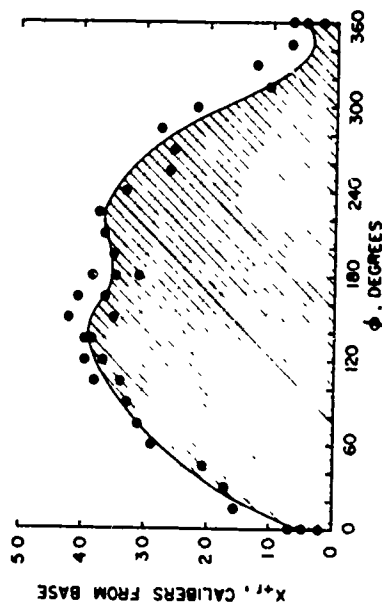
$M=3, \Omega=0 \text{ RPM}, \alpha=4^\circ$



$M=3, \Omega=8000 \text{ RPM}, \alpha=4^\circ$



$M=3, \Omega=16000 \text{ RPM}, \alpha=4^\circ$



$M=3, \Omega=24000 \text{ RPM}, \alpha=4^\circ$

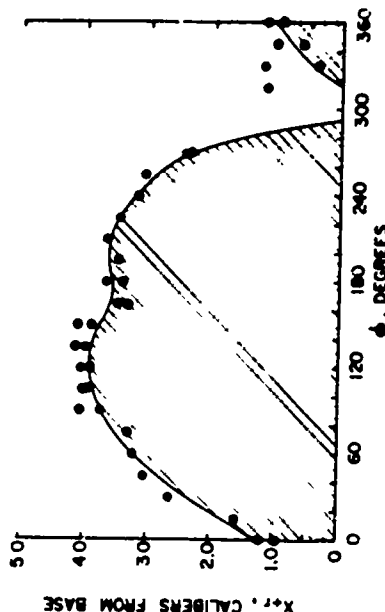


Figure 7. Concluded

b. $M=3, \alpha=4^\circ$

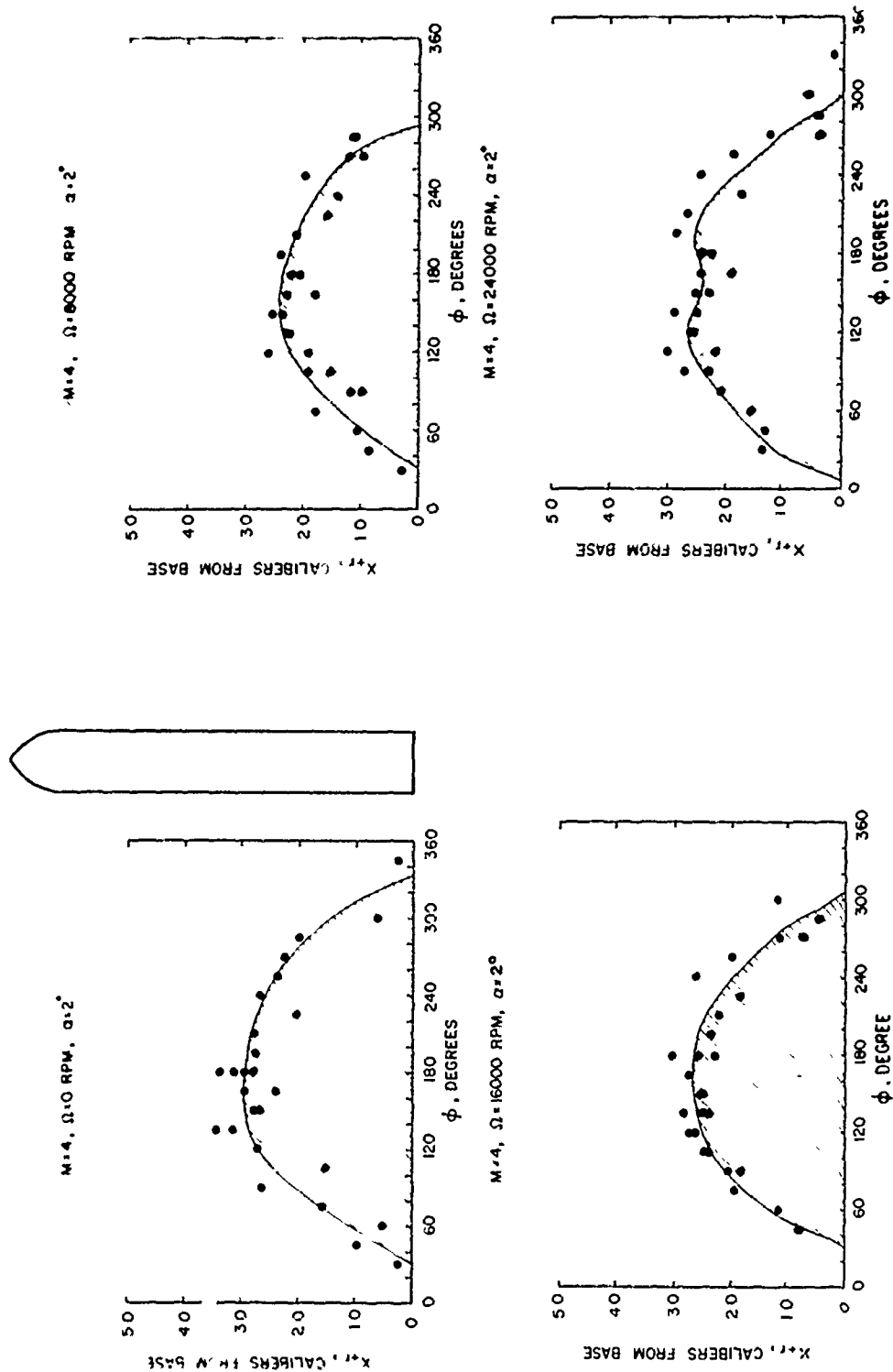


Figure 8. Boundary Layer Transition Data

a. $M = 4, \alpha = 2^\circ$

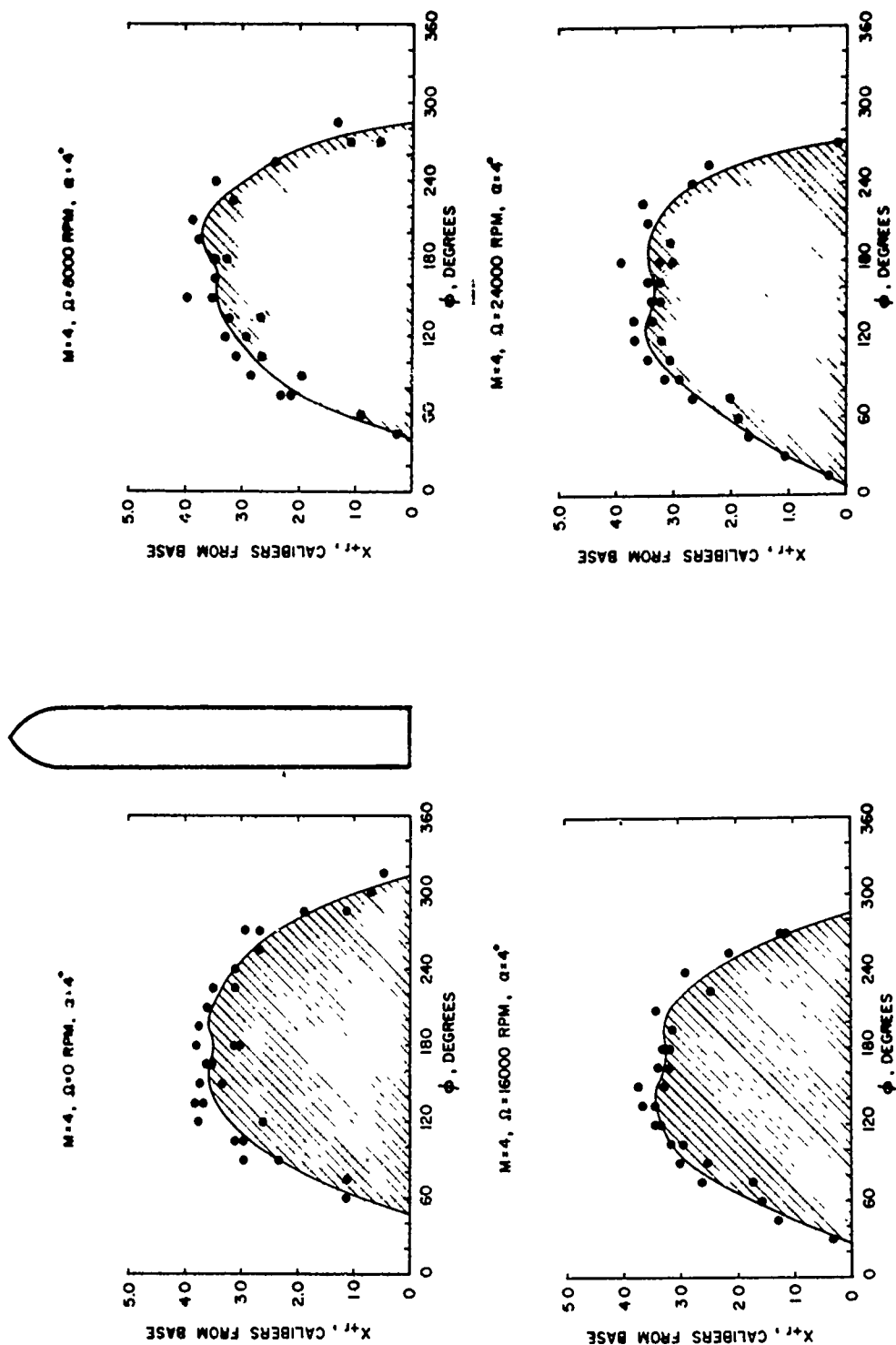


Figure 8. Concluded

b. $M = 4, \alpha = 4^\circ$

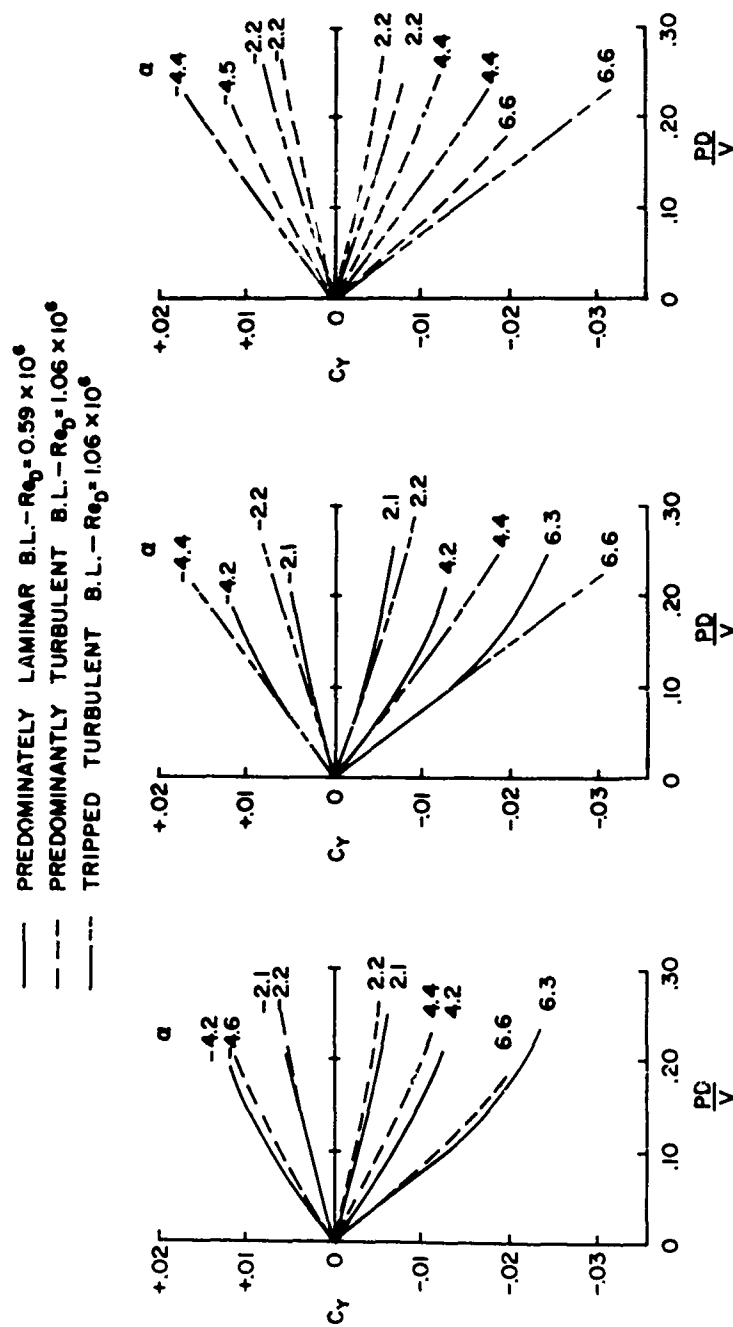


Figure 9. Comparison of Magnus Force Measurements for Different Boundary Layer Configurations, $N = 3$

SYM.	RUN NUMBER	MACH	CONFIG.	ALPHA	$Re_D \times 10^6$
■	137	2.00	10.000	10.80	0.63
■	136	2.00	10.000	8.71	0.63
▲	135	2.00	10.000	6.56	0.63
▼	134	2.00	10.000	4.37	0.63
+	133	2.00	10.000	2.18	0.63
x	139	2.00	10.000	-2.18	0.63
•	140	2.00	10.000	-4.37	0.63

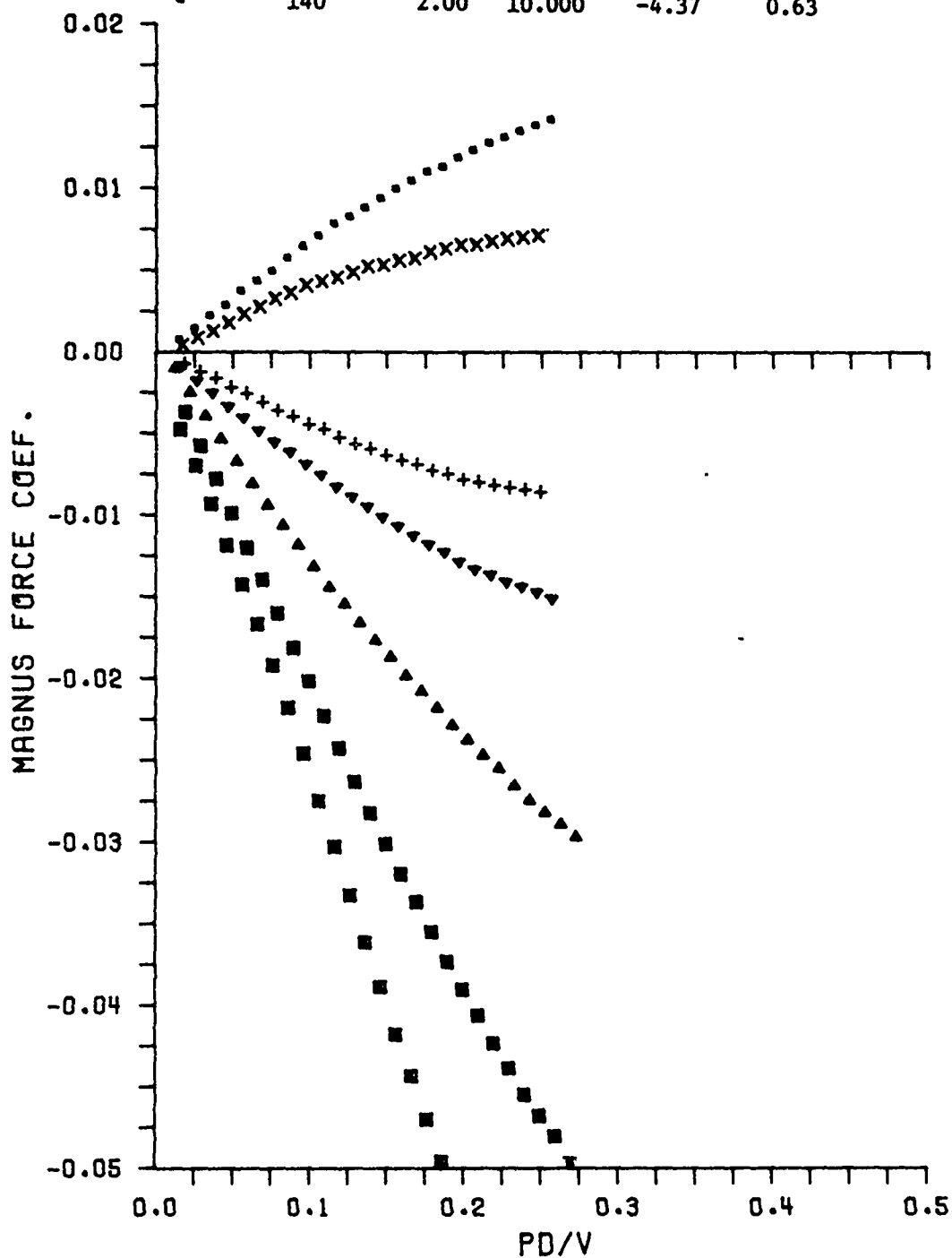


Figure 10a. Magnus Force Measurements for Low p_0 , Natural Boundary Layer Transition--Predominantly Laminar Boundary Layer, $M = 2$

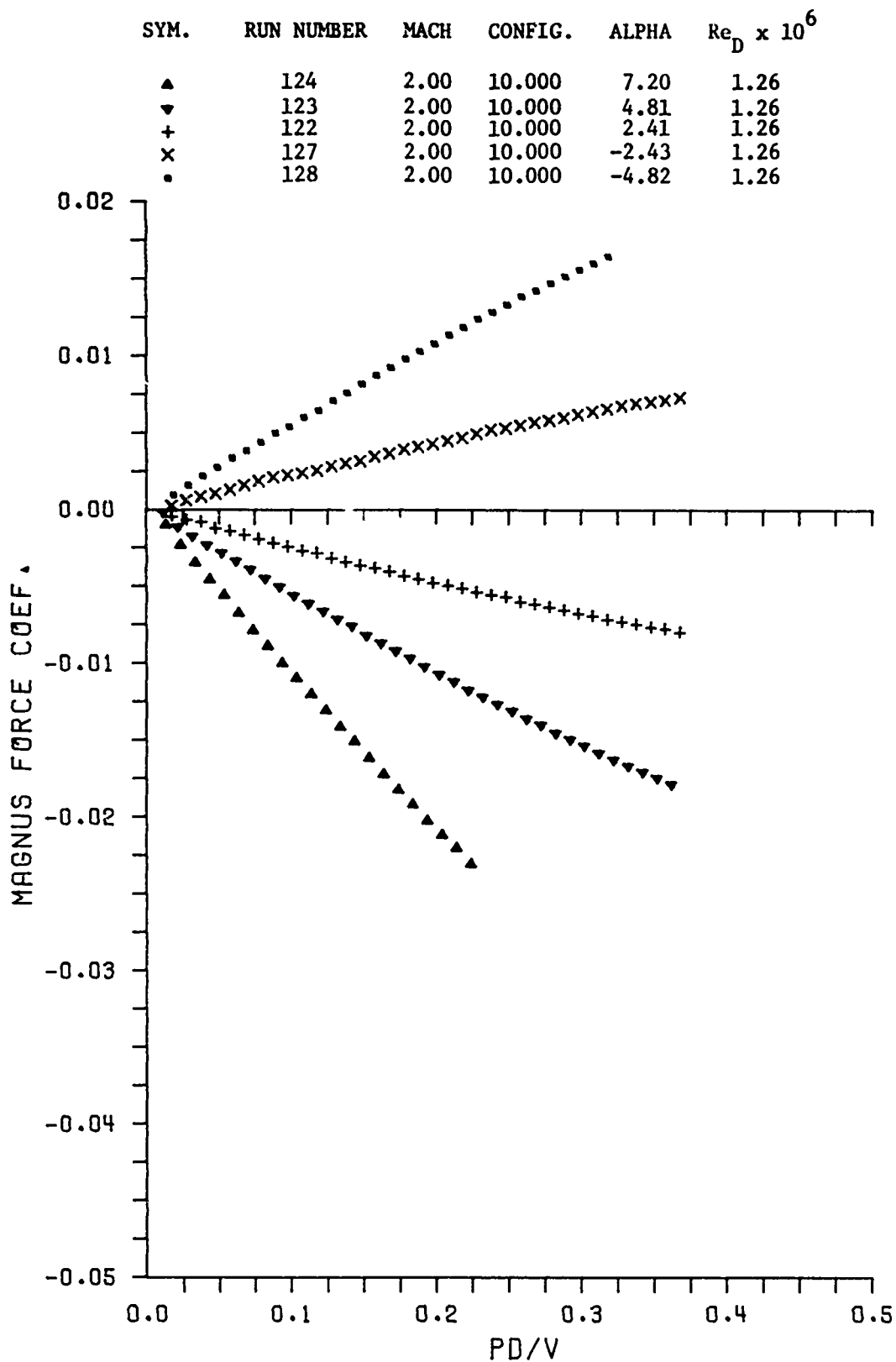


Figure 10b. Magnus Force Measurements for High p_0 , Natural Boundary Layer Transition--Comparable Regions of Laminar and Turbulent Boundary Layer, $M = 2$

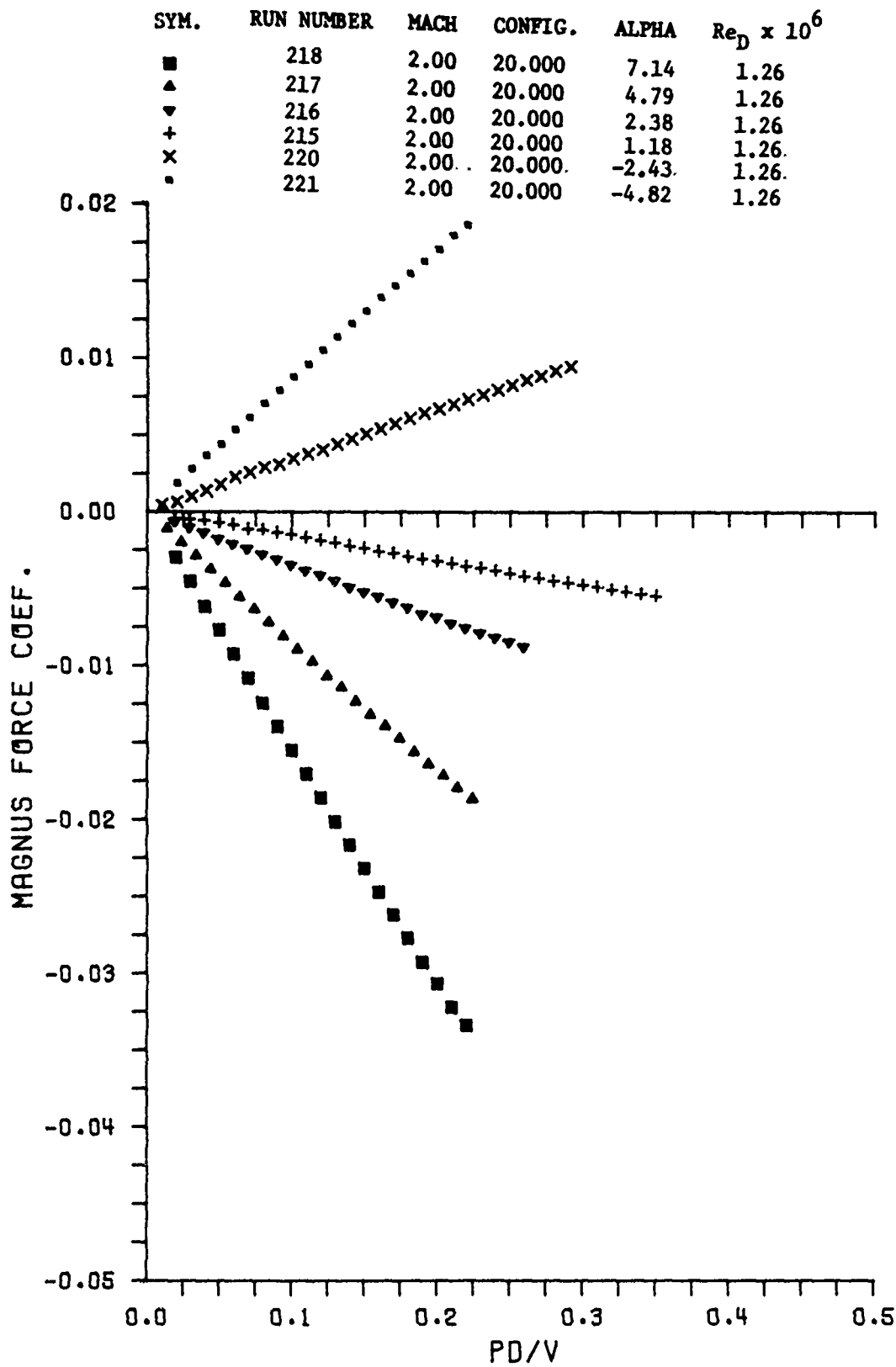


Figure 10c. Magnus Force Measurements for High p_o ,
Tripped Turbulent Boundary Layer, $M = 2$

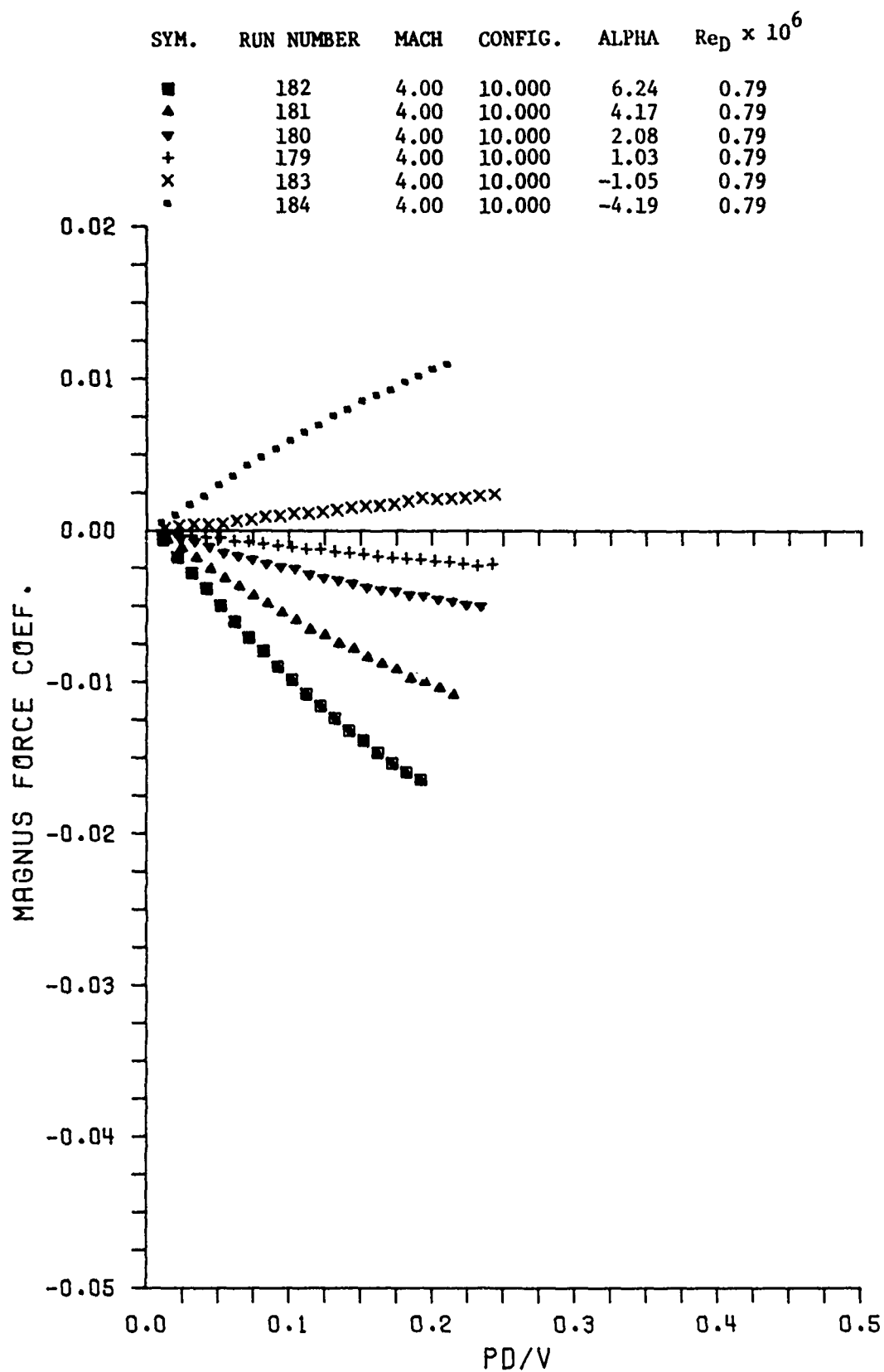


Figure 11a. Magnus Force Measurements for Low p_0 , Natural Boundary Layer Transition--Predominantly Laminar Boundary Layer, $M = 4$

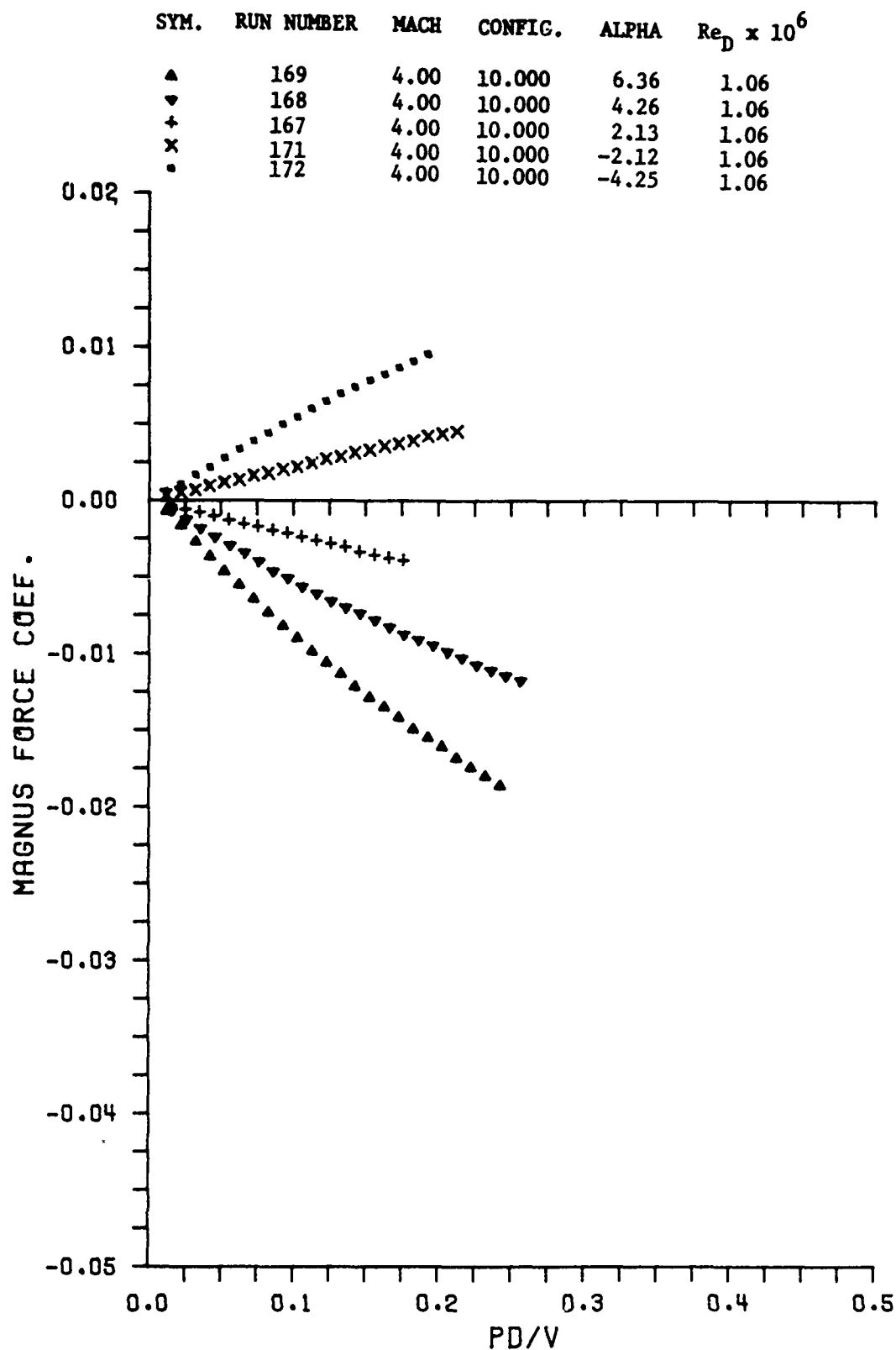


Figure 11b. Magnus Force Measurements for High p_0 , Natural Boundary Layer Transition--Comparable Regions of Laminar and Turbulent Boundary Layer, $M = 4$

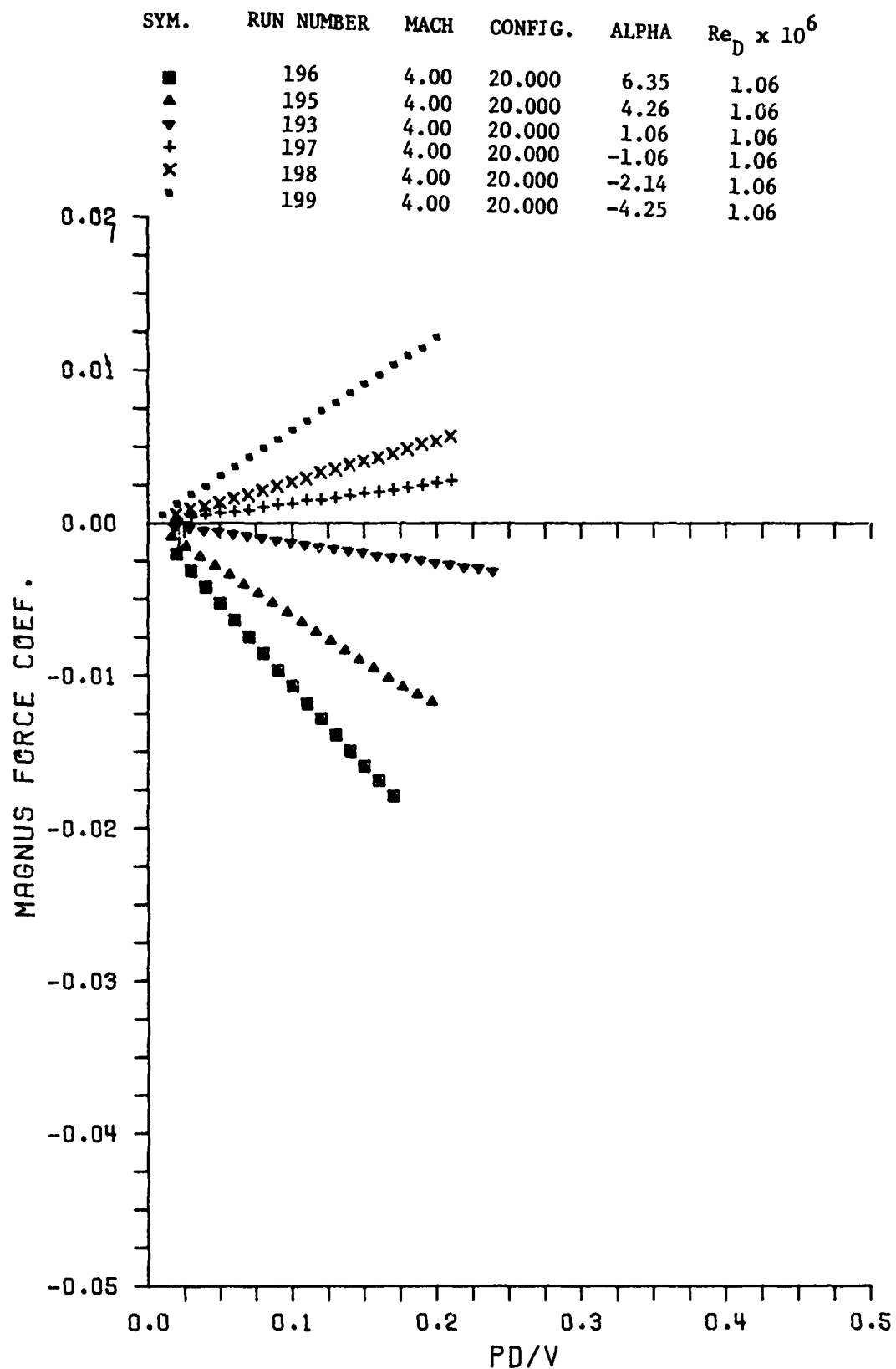


Figure 11c. Magnus Force Measurements for High p_o ,
Tripped Turbulent Boundary Layer, $M = 4$

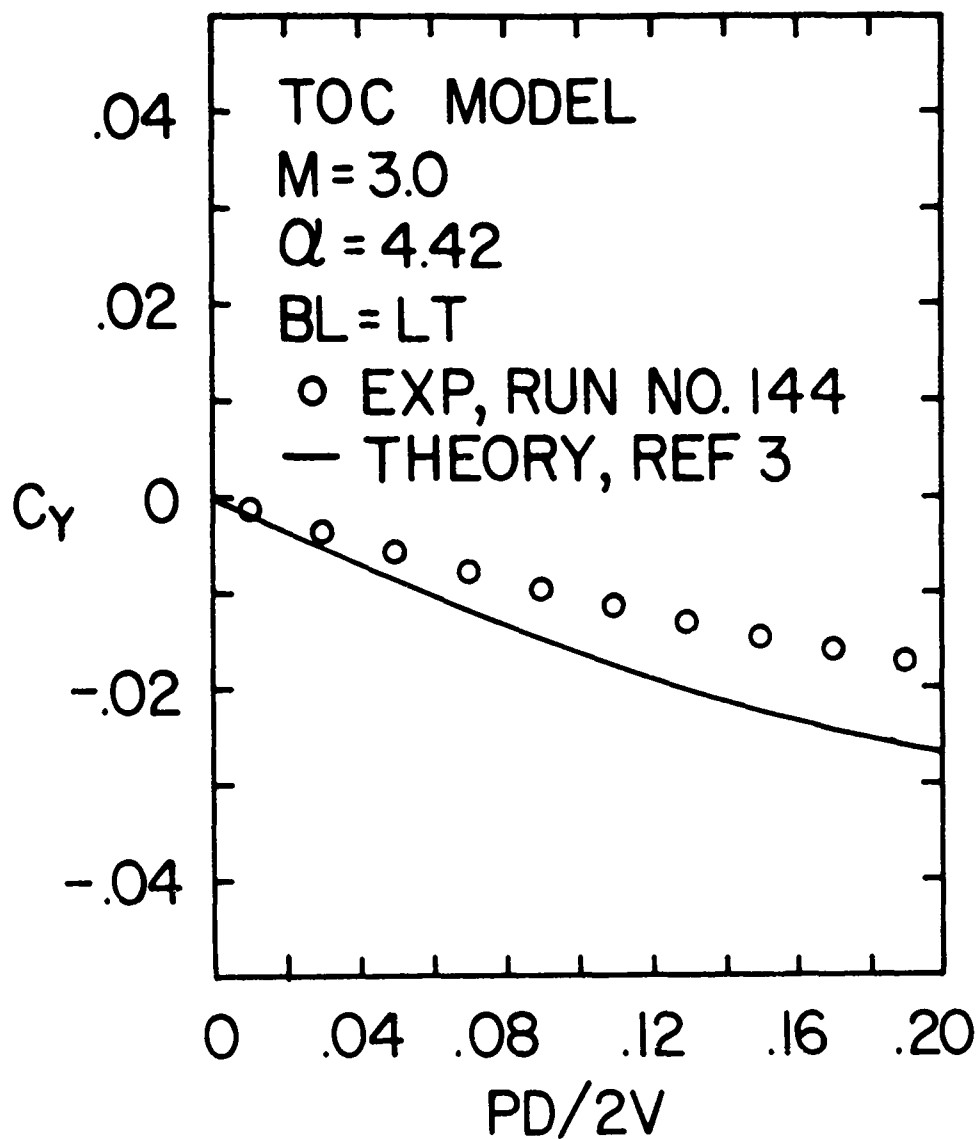


Figure 12. Comparison of Magnus Force Measurements to Theory, High p_0

a. Natural Boundary Layer Transition, $M = 3$, $\alpha = 4.42^\circ$

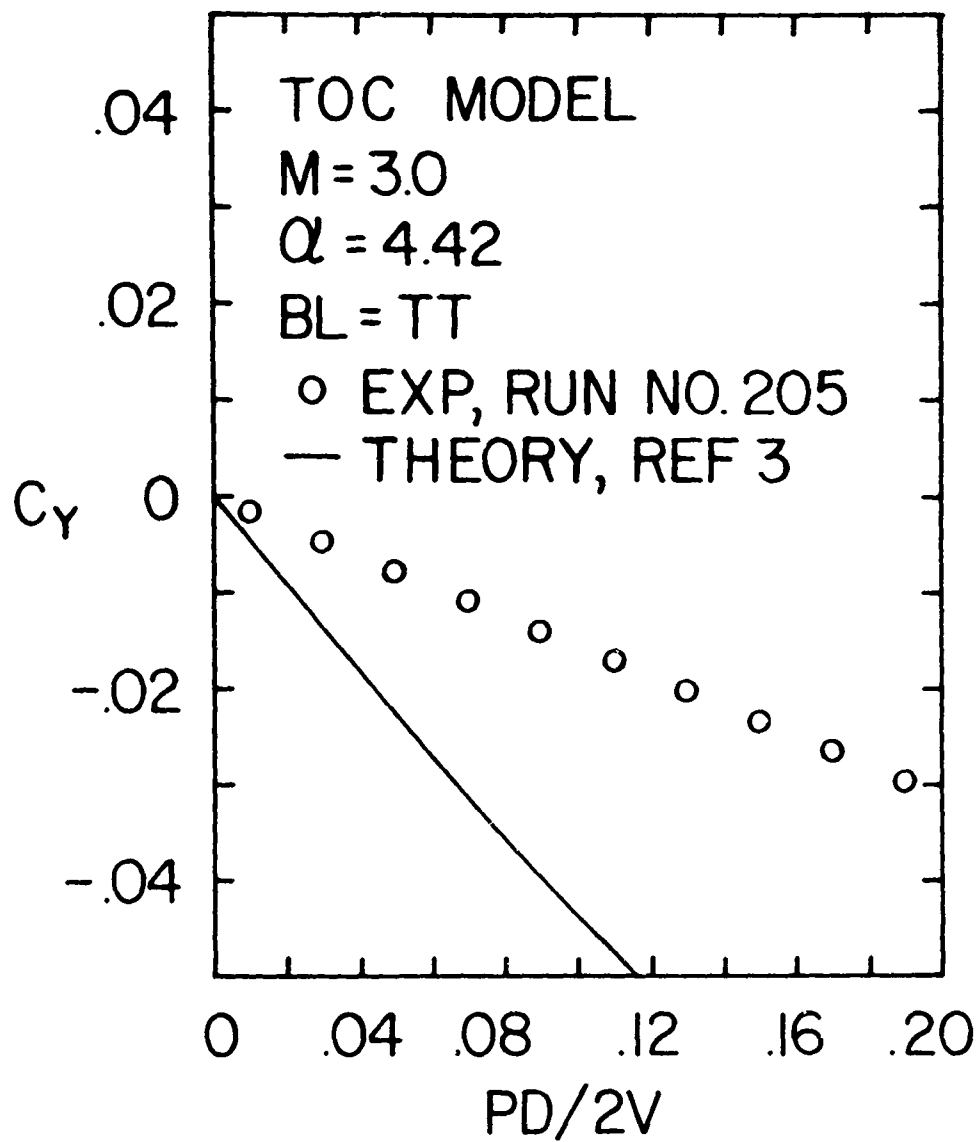


Figure 12. Concluded

b. Tripped Turbulent Boundary Layer, $M = 3$, $\alpha = 4.42^\circ$

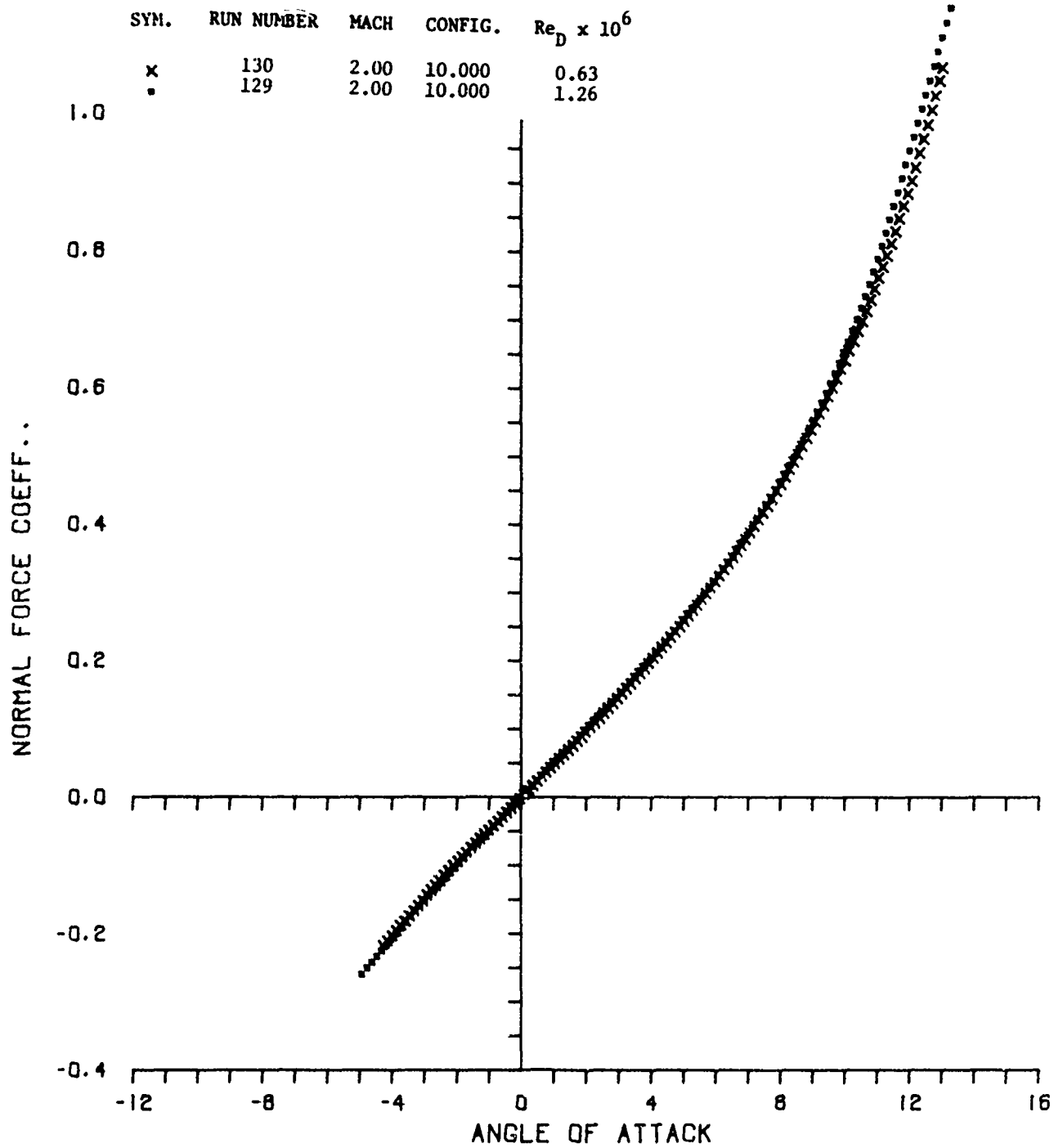
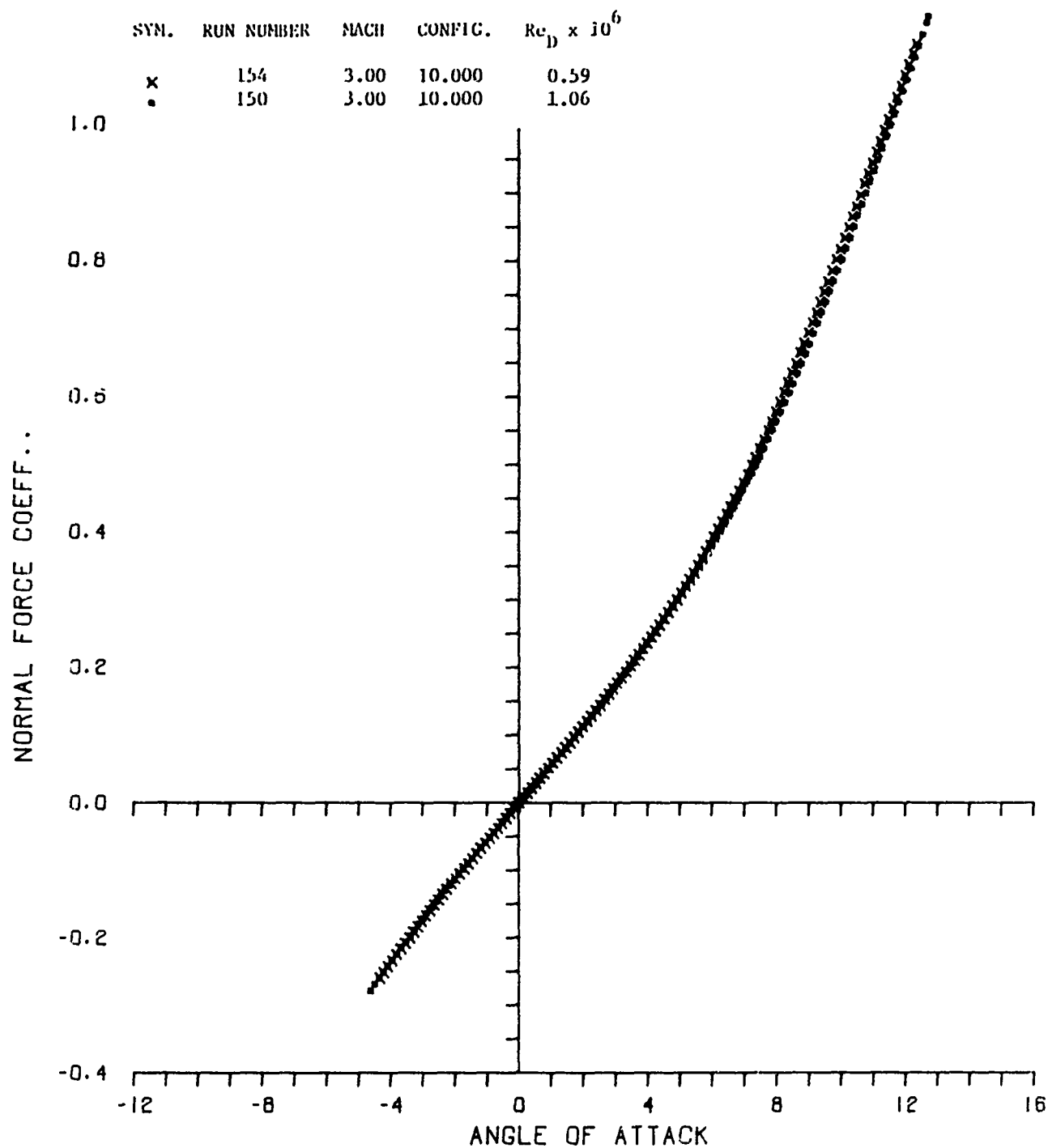


Figure 13. Normal Force Data

a. $M = 2$



SYM.	RUN NUMBER	MACH	CONFIG.	$Re_D \times 10^6$
▼	200	4.00	20.000	1.06
+	185	4.00	10.000	0.79
x	173	4.00	10.000	0.79
•	164	4.00	10.000	1.06

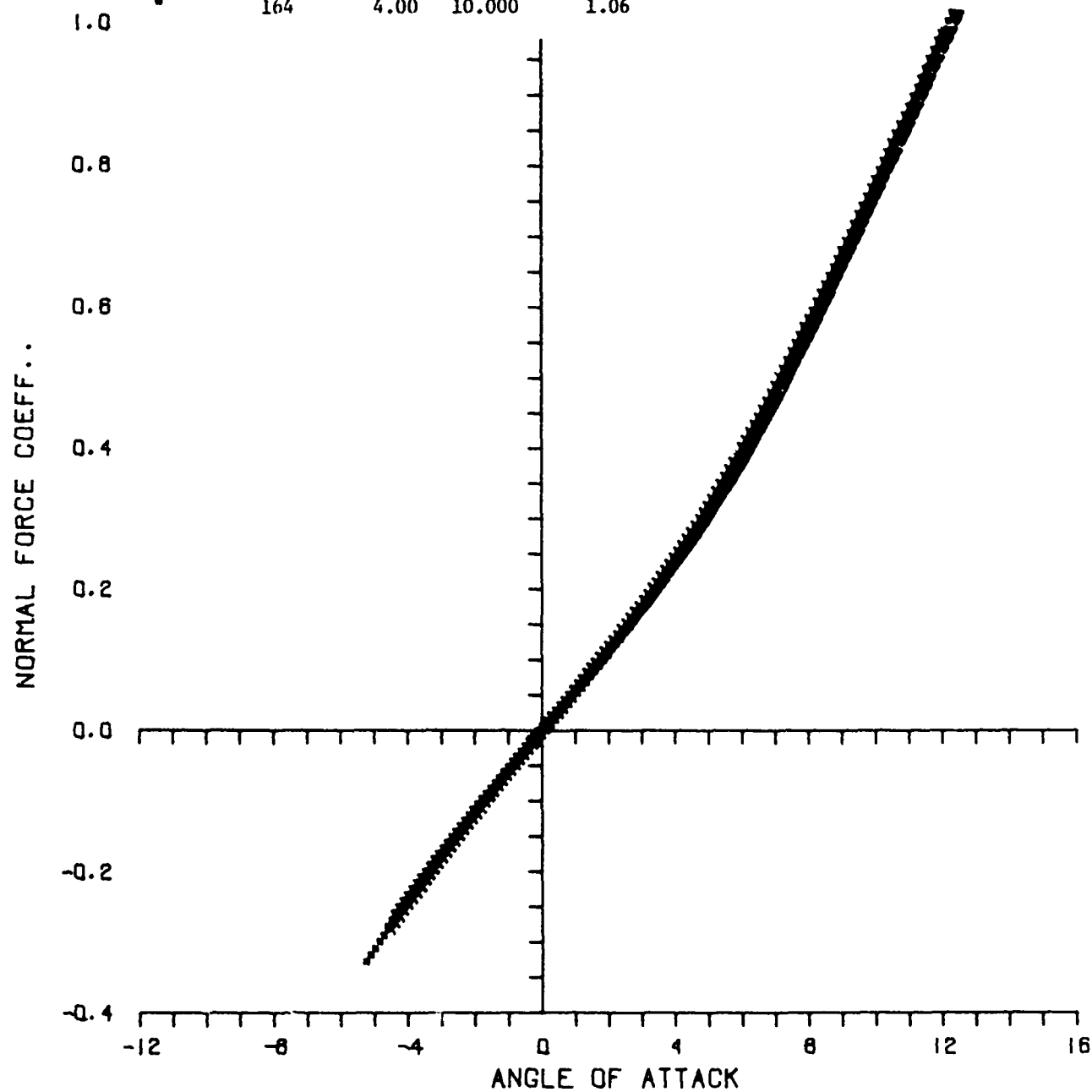


Figure 13. Concluded

c. $M = 4$

REFERENCES

1. W. B. Sturek, "Boundary Layer Studies on a Spinning Cone," BRL Report No. 1649, U.S. Army Ballistic Research Laboratories, Aberdeen Proving Ground, Maryland, May 1973. AD 762564.
2. J. C. McMullen, "Wind Tunnel Testing Facilities at the Ballistic Research Laboratories," BRL Memorandum Report No. 1292, U.S. Army Ballistic Research Laboratories, Aberdeen Proving Ground, Maryland, July 1960. AD 244180.
3. H. R. Vaughn and G. E. Reis, "A Magnus Theory for Bodies of Revolution," SC-RR-72 0537, Sandia Laboratories, Albuquerque, New Mexico, January 1973; also, *AIAA Journal*, Vol. 11, No. 10, p. 1396, October 1973.

LIST OF SYMBOLS

ALPHA	angle of attack, degrees
BL = LT	natural transition, laminar and turbulent boundary layer
BL = TT	tripped turbulent boundary layer
C_M	pitching moment coefficient, $M_N/qSD\ell$, referenced to model base
C_N	normal force coefficient, F_N/qS
C_Y	side (Magnus) force coefficient, F_Y/qS
C_{YM}	side (Magnus) moment coefficient, $M_Y/qSD\ell$, referenced to model base
D	diameter of base of model, .0508 m
F_N	normal force
F_Y	side (Magnus) force
ℓ	model length, 7 calibers = .3556 m
M_N	pitching moment, referenced to model base
M_Y	side (Magnus) moment, referenced to model base
p_o	tunnel total pressure, Pascals
P	spin rate of model, radians per second
PD/V	non-dimensional spin rate
q	free stream dynamic pressure, $\frac{1}{2} \rho V^2$
Re_D	Reynolds number based on model diameter and free stream properties
Re_ℓ	Reynolds number based on model length and free stream properties
S	reference area, $\pi D^2/4$

LIST OF SYMBOLS (Continued)

T_o	tunnel total temperature, degrees Kelvin
V	free stream velocity, cm per second
X_{tr}	location of boundary layer transition, calibers from model base
α	angle of attack, degrees
ρ	free stream density
ϕ	azimuthal position, equals zero on windward ray, see Figure 5
ω	spin rate of model, revolutions per minute

DISTRIBUTION LIST

<u>No. of Copies</u>	<u>Organization</u>	<u>No. of Copies</u>	<u>Organization</u>
12	Commander Defense Documentation Center ATTN: DDC-TCA Cameron Station Alexandria, VA 22314	1	Director US Army Air Mobility Research & Development Laboratory Ames Research Center ATTN: SAVDL-D Moffett Field, CA 94035
2	Commander US Army Materiel Command ATTN: AMCDMA, N. Klein J. Bender 5001 Eisenhower Avenue Alexandria, VA 22333	2	Commander US Army Electronics Command ATTN: AMSEL-CT/L, Mr. B. Louis AMSEL-RD Fort Monmouth, NJ 07703
1	Commander US Army Materiel Command ATTN: AMCRD, BG H. A. Griffith 5001 Eisenhower Avenue Alexandria, VA 22333	3	Commander US Army Missile Command ATTN: AMSMI-R AMXMI-RDK Mr. R. Deep Mr. R. Becht Redstone Arsenal, AL 35809
1	Commander US Army Materiel Command ATTN: AMCRD-T 5001 Eisenhower Avenue Alexandria, VA 22333	1	Commander US Army Tank-Automotive Command ATTN: AMSTA-RHFL Warren, MI 48090
1	Commander US Army Materiel Command ATTN: AMCRD-R 5001 Eisenhower Avenue Alexandria, VA 22333	2	Commander US Army Mobility Equipment Research & Development Center ATTN: Tech Docu Ctr, Bldg. 315 AMSME-RZT Fort Belvoir, VA 22060
1	Commander US Army Materiel Command ATTN: AMCRD-MT 5001 Eisenhower Avenue Alexandria, VA 22333	1	Commander US Army Armament Command Rock Island, IL 61202
1	Commander US Army Aviation Systems Command ATTN: AMSAV-E 12th & Spruce Streets St. Louis, MO 63166	4	Commander US Army Picatinny Arsenal ATTN: SARPA-AD Mr. S. Wasserman SARPA-FR-S-A Mr. A. Loeb Mr. D. Mertz Mr. E. Falkowski Dover, NJ 07801

DISTRIBUTION LIST

<u>No. of Copies</u>	<u>Organization</u>	<u>No. of Copies</u>	<u>Organization</u>
1	Commander US Army Jefferson Proving Ground ATTN: STEJP-TD-D Madison, IN 47250	1	Commander US Naval Surface Weapons Center ATTN: Dr. W. Kemper Dahlgren, VA 22448
1	Commander US Army Harry Diamond Labs. ATTN: AMXDO-TI 2800 Powder Mill Road Adelphi, MD 20783	6	Commander US Naval Ordnance Laboratory ATTN: Code 031, Mr. K. Lobb Code 312, Mr. S. Hastings Code 312, Mr. F. Regan Code 313, Mr. R. Lee Mr. W. Yanta Mr. R. Voisinet Silver Spring, MD 20910
1	Commander US Army Materials and Mechanics Research Center ATTN: AMXMR-ATL Watertown, MA 02172	1	AFATL (DLR) Eglin AFB Florida 32542
1	Commander US Army Natick Laboratories ATTN: AMXRE, Dr. D. Sieling Natick, MA 01762	1	AFATL (DLRD) Eglin AFB Florida 32542
1	Commander US Army Research Office ATTN: CRD-AA-EH P.O. Box 12211 Research Triangle Park, NC 27709	1	AFATL (DLRV) Eglin AFB Florida 32542
3	Commander US Naval Air Systems Command ATTN: AIR-604 Washington, DC 20360	1	ARL (Dr. J. S. Shang Bldg. 450, Area B) Wright-Patterson AFB Ohio 45433
3	Commander US Naval Ordnance Systems Cmd ATTN: ORD-0632 ORD-035 ORD-5524 Washington, DC 20360	2	Director National Aeronautics and Space Administration Ames Research Center ATTN: C. C. Horstman William C. Rose Moffett Field, CA 94035
1	Commander US Naval Ship Research and Development Center ATTN: Dr. S. de los Santos Aerodynamics Lab. Washington, DC 20007	2	Director National Aeronautics and Space Administration Langley Research Center ATTN: MS 185, Tech Library MS 161, Mr. D. Bushnell Langley Station Hampton, VA 23365

DISTRIBUTION LIST

<u>No. of Copies</u>	<u>Organization</u>	<u>No. of Copies</u>	<u>Organization</u>
1	Director National Aeronautics and Space Administration Lewis Research Center ATTN: MS 60-3, Tech Library 21000 Brookpark Road Cleveland, OH 44135	1	Lockheed Missiles and Space Company ATTN: Tech Information Center 3251 Hanover Street Palo Alto, CA 94304
2	Director Jet Propulsion Laboratory ATTN: Mr. B. Dayman Technical Library 4800 Oak Grove Drive Pasadena, CA 91103	1	Douglas Aircraft Co. McDonnell-Douglas Corp. ATTN: Dr. Tuncer Cebeci 3855 Lakewood Blvd. Long Beach, CA 90801
2	ARO, Inc. ATTN: Technical Library Arnold AFS Tennessee 37389	1	McDonnell-Douglas Aircraft Corporation Missiles and Space Systems Division ATTN: Aerodynamics Branch 3000 Ocean Park Blvd. Santa Monica, CA 90405
1	AVCO Systems Division ATTN: Dr. B. Reeves 201 Lowell Street Wilmington, MA 01887	1	Sandia Laboratories ATTN: Dr. F. G. Blottner P.O. Box 5800 Albuquerque, NM 87115
1	Calspan Corporation ATTN: Mr. J. Andes, Head Transonic Tunnel Dept. P.O. Box 235 Buffalo, NY 14221	1	United Aircraft Corporation Research Laboratories ATTN: Library East Hartford, CT 06108
1	General Dynamics ATTN: Research Library 2246 P.O. Box 748 Fort Worth, TX 76101	2	California Institute of Technology Aeronautics Department ATTN: Prof. H. Liepmann Prof. W. Behrens 1201 East California Blvd. Pasadena, CA 91102
1	General Electric Company ATTN: Dr. H. T. Nagamatsu Research and Development Laboratory (Comb. Bldg.) Schenectady, NY 12301	1	California Institute of Technology Guggenheim Aeronautical Lab. ATTN: Technical Library Pasadena, CA 91104

DISTRIBUTION LIST

<u>No. of Copies</u>	<u>Organization</u>	<u>No. of Copies</u>	<u>Organization</u>
1	Cornell University Graduate School of Aero. Engineering ATTN: Prof. W. R. Sears Ithaca, NY 14850	1	Princeton University James Forrestal Research Center Gas Dynamics Laboratory ATTN: Prof. S. Bogdonoff Princeton, NJ 08540
1	Illinois Institute of Technology ATTN: Dr. M. V. Morkovin 3300 South Federal Chicago, IL 60616	1	Southwest Research Institute Applied Mechanics Reviews 8500 Culebra Road San Antonio, TX 78228
2	The Johns-Hopkins University ATTN: Prof. S. Corrsin Prof. L. Kovasznay Baltimore, MD 21218	1	University of California-- San Diego Department of Aerospace and Mechanical Engr. Sciences ATTN: Prof. P. A. Libby La Jolla, CA 92037
3	Massachusetts Institute of Technology ATTN: Technical Library Prof. E. Covert Prof. C. Haldeman 77 Massachusetts Avenue Cambridge, MA 02139	1	University of California Department of Mechanical Engr. ATTN: Prof. H. A. Dwyer Davis, CA 95616
1	New York University University Heights ATTN: Prof. V. Zaakay New York, NY 10453	1	University of Delaware Mechanical and Aerospace Engineering Department ATTN: Dr. J. E. Danberg Newark, DE 19711
1	Director Guggenheim Aerospace Labs. New York University New York Heights New York, NY 10053	3	University of Maryland ATTN: Prof. A. W. Sherwood Dept. of Aero. Engr. Dr. S. I. Pai, Inst. for Fluid Dynamics and Applied Mathematics Dr. W. L. Melnik Dept. of Aero. Engr. College Park, MD 20740
1	Notre Dame University ATTN: Department of Aerospace Engineering South Bend, IN 46556	1	University of Michigan Department of Aeronautical Engineering ATTN: Dr. A. Kuethe East Engineering Building Ann Arbor, MI 48104
1	Ohio State University Department of Aeronautical and Astronautical Engineering ATTN: Technical Library Columbus, OH 43210		

DISTRIBUTION LIST

<u>No. of Copies</u>	<u>Organization</u>
1	University of Virginia Department of Aerospace Engineering and Engineering Physics ATTN: Prof. I. Jacobson Charlottesville, VA 22904
1	University of Washington Department of Mechanical Engineering ATTN: Prof. M. E. Childs Seattle, WA 98195
2	Virginia Polytechnic Institute Department of Aerospace Engineering ATTN: Prof. J. A. Schetz Prof. C. H. Lewis Blacksburg, VA 24061

Aberdeen Proving Ground

Marine Corps Ln Ofc
Director, USAMSAA